Atmos. Chem. Phys., 25, 7111–7136, 2025
https://doi.org/10.5194/acp-25-7111-2025

Atmospheric Chemistry and Physics
Open Access
EGU

Research article

Drivers of change in peak-season surface ozone concentrations and impacts on human health over the historical period (1850–2014)

Steven T. Turnock[1,2], Dimitris Akritidis[3,4], Larry Horowitz[5], Mariano Mertens[6], Andrea Pozzer[3,7], Carly L. Reddington[8], Hantao Wang[9], Putian Zhou[10], and Fiona O'Connor[1,11]

[1]Met Office Hadley Centre, Exeter, UK
[2]University of Leeds Met Office Strategic (LUMOS) Research Group, University of Leeds, Leeds, UK
[3]Atmospheric Chemistry Department, Max Planck Institute for Chemistry, Mainz, Germany
[4]Department of Meteorology and Climatology, School of Geology, Aristotle University of Thessaloniki, Thessaloniki, Greece
[5]NOAA Geophysical Fluid Dynamics Laboratory, Princeton, NJ, USA
[6]Deutsches Zentrum für Luft- und Raumfahrt (DLR), Institut für Physik der Atmosphäre, Oberpfaffenhofen, Germany
[7]Climate and Atmosphere Research Center, The Cyprus Institute, 1645 Nicosia, Cyprus
[8]Institute for Climate and Atmospheric Science (ICAS), School of Earth and Environment, University of Leeds, Leeds, UK
[9]Department of Environmental Sciences and Engineering, University of North Carolina at Chapel Hill, Chapel Hill, North Carolina 27599, USA
[10]Institute for Atmospheric and Earth System Research (INAR), University of Helsinki, Helsinki, Finland
[11]Department of Mathematics and Statistics, Global Systems Institute, University of Exeter, Exeter, UK

Correspondence: Steven T. Turnock (steven.turnock@metoffice.gov.uk)

Received: 30 August 2024 – Discussion started: 14 October 2024
Revised: 19 February 2025 – Accepted: 8 April 2025 – Published: 10 July 2025

Abstract. Elevated concentrations of ozone at the surface can lead to poor air quality and increased risks to human health. There have been large increases in surface ozone over the historical period associated with socio-economic development. Here, the change in peak-season ozone (OSDMA8) is estimated for the first time using hourly surface ozone output from three CMIP6 models over the 1850 to 2014 period. Additional results are obtained from one model to quantify the impact from different drivers of ozone formation, including anthropogenic emissions of ozone and aerosol precursors, stratospheric ozone, and climate change. The peak-season ozone concentrations are used to calculate the risk to human health, in terms of the attributable fraction metric (the percentage of deaths from COPD – chronic obstructive pulmonary disease – associated with long-term exposure to elevated ozone concentrations). OSDMA8 concentrations are simulated to increase by more than 50 % across northern mid-latitude regions over the historical period, mainly driven by increases in anthropogenic emissions of NO_x and global CH_4 concentrations. Small contributions are made from changes in other anthropogenic precursor emissions (CO and non-CH_4 volatile organic compounds; VOCs), aerosols, stratospheric ozone and climate change. The proportion of the global population exposed to OSDMA8 concentrations above the theoretical minimum risk exposure level (32.4 ppb) increased from < 20 % in 1855 to > 90 % in 2010. This has also increased the risk to human health mortality due to COPD from long-term ozone exposure by up to 20 % across Northern Hemisphere regions in the present day. Like for OSDMA8 concentrations, the drivers of the increase in the ozone health risks are attributed mainly to changes in NO_x and global CH_4. Fixing anthropogenic NO_x emissions at 1850 values can eliminate the risk to human health from long-term ozone exposure in the near-

present-day period. Understanding the historical drivers of ozone concentrations and their risk to human health can help to inform the development of future pathways that reduce this risk.

1 Introduction

Ozone is a greenhouse gas in the troposphere and classified as a secondary air pollutant at the Earth's surface, influencing both the Earth's radiative balance and regional air quality (Szopa et al., 2021). It is formed by photochemical reactions involving nitrogen oxides (NO_x), carbon monoxide (CO) and volatile organic compounds (VOCs, including CH_4) (Lelieveld and Dentener, 2000). Perturbations to the emissions associated with these precursors from both anthropogenic and natural sources can therefore alter net ozone production rates. In addition, the formation of ozone can also be impacted by geographical location and meteorological conditions such as temperature and photolysis rates (Monks et al., 2015). Furthermore, ozone concentrations at the surface are also affected by chemical destruction, surface deposition processes (Mills et al., 2018), hemispheric transport (Liang et al., 2018) and the downward transport of ozone from the stratosphere (Stohl et al., 2003; Chen et al., 2024), the stratosphere–troposphere exchange (STE). In air pollution episodes, exposure to elevated surface concentrations of ozone can lead to impacts on human health associated with respiratory diseases such as chronic obstructive pulmonary disease (COPD) (Pozzer et al., 2023). The Global Burden of Disease (GBD) study in 2019 estimated that long-term exposure to concentrations of ozone resulted in 365 000 annual mortalities from COPD (Murray et al., 2020), with a recent revision by the GBD 2021 assessment to 490 000 annual mortalities in 2021 from COPD (GBD 2021 Risk Factors Collaborators, 2024). Therefore, ozone pollution represents a large current risk to the health of a population, requiring an understanding of the factors controlling changes in concentrations.

Surface ozone concentrations are understood to have rapidly increased throughout the 20th century due to industrial development and increased anthropogenic emissions of ozone precursors. Even with the uncertainties surrounding early measurements of surface ozone at the end of the 19th and beginning of the 20th century, ozone concentrations are observed to have increased across the temperate and polar regions of the Northern Hemisphere by 30 % to 70 % (approximately 10 to 16 ppb) since the start of the 20th century (Tarasick et al., 2019). Previous multi-model intercomparison exercises have simulated the historical change in annual or seasonal mean tropospheric and surface ozone concentrations. In both the fifth and sixth phases of the Coupled Model Intercomparison Project (CMIP5 and CMIP6), the historical change in annual mean global surface ozone concentrations from 1850 to 2000 was simulated to be in agreement at 10 to 11 ppb (Young et al., 2013; Turnock et al., 2020). Simulated historical changes in annual mean surface ozone were larger at 15 to 20 ppb across Northern Hemisphere mid-latitude regions in both CMIP5 and CMIP6, although some regions like South and East Asia showed large inter-model diversity. However, in both phases of CMIP, the simulated historical changes in surface ozone concentrations were in part dominated by the large uncertainty in the simulated pre-industrial values of 1850 (Young et al., 2013; Turnock et al., 2020). Evaluating historical changes in surface ozone concentrations is limited by the availability and reliability of observations with a sufficiently long record. Sufficient observation data are available over the last 5 to 6 decades across regions within the northern mid-latitudes (North America, Europe and Japan) and show that both CMIP5 and CMIP6 models underestimated the recent rapid increase in surface ozone concentrations that occurred over these regions (Young et al., 2018; Parrish et al., 2014, 2021). However, the CMIP6-model-simulated long-term change in ozone concentrations shows good agreement when compared to the observed trend at only remote observation locations (Griffiths et al., 2021). Evaluation of the present-day simulation of ozone concentrations in CMIP5 (2000) and CMIP6 (2005 to 2014 mean) shows that both generations of chemistry climate models are able to represent the spatial and seasonal distributions of ozone but overestimate the absolute concentrations at the surface compared to ground-based observations collected as part of the Tropospheric Ozone Assessment Report (TOAR) (Young et al., 2018; Turnock et al., 2020).

Dedicated model simulations allow for the studies focusing on the drivers of historical ozone changes. Generally, the most important drivers of historical ozone changes have been increases in anthropogenic emissions, especially emissions of NO_x (e.g. Lelieveld and Dentener, 2000; Fiore et al., 2009; Young et al., 2013; Turnock et al., 2018), with different emission sectors having different effects on ozone due to different trends and ozone production efficiency (Dahlmann et al., 2011; Mertens et al., 2024). Besides increases in NO_x emissions, the increase in methane is also an important driver (Wild et al., 2012; Iglesias-Suarez et al., 2018; Mor-

genstern et al., 2018). Moreover, changes in aerosols (Xing et al., 2017), emissions of N_2O and ozone-depleting substances (ODSs) drive changes in tropospheric ozone (Morgenstern et al., 2018; Iglesias-Suarez et al., 2018; Zeng et al., 2022). Changes in climate via temperature, water vapour and radiation can also influence surface ozone concentrations, with increases and decreases generally anticipated in polluted and unpolluted regions, respectively (Schnell et al., 2016; Fortems-Cheiney et al., 2017; Fu and Tian, 2019; Zanis et al., 2022). Uncertainties in various processes, such as the description of natural emissions which differ in various models, however, hinder a consistent quantification of ozone drivers among various models (Archibald et al., 2020a).

Until lately, global estimates of ozone-attributable health impacts were based on outputs from global atmospheric-chemistry models providing surface ozone concentrations in sufficient spatio-temporal distributions for ozone exposure assessments (Anenberg et al., 2010; Lim et al., 2012; Lelieveld et al., 2015; Fang et al., 2013; Silva et al., 2013; Forouzanfar et al., 2015; Silva et al., 2016; Cohen et al., 2017; Malley et al., 2017; Liang et al., 2018; Lelieveld et al., 2020). However, as part of the first phase of TOAR, Fleming et al. (2018) provided an assessment of recent changes in relevant ozone health metrics calculated from observations, showing recent reductions since 2000 across northern mid-latitude regions (North America, Europe and East Asia). More recently, the synergistic use of in situ ozone measurements and model outputs through data fusion has made it possible to assess ozone-related health effects (Murray et al., 2020; Malashock et al., 2022) based on observational-based gridded ozone datasets (DeLang et al., 2021; Becker et al., 2023). Over the previous years, different ozone exposure metrics were applied, according to the adopted coefficients from relevant cohort studies. The exposure response function (ERF) for ozone is actually a mathematical formula expressing the relative risk (RR) of a disease as a function of ozone abundance. Pope et al. (2002) and Ostro (2004) introduced a log-linear ERF based on epidemiological findings, while later a log–log ERF approach was proposed (Cohen et al., 2005). In the GBD 2019 report (Murray et al., 2020), a log-linear ERF was used, introducing an ozone exposure metric based on the ozone season daily maximum 8 h mixing ratio (OSDMA8). Malashock et al. (2022), using the observation-based gridded OSDMA8 dataset of DeLang et al. (2021) and the GBD2019 approach for mortality calculations, reported 423 000 ozone-related deaths worldwide for the year 2019, accounting for all respiratory diseases. The review by Pozzer et al. (2023) showed that global estimates of mortality from long-term exposure to ozone have a large range from 142 000 per year from COPD to 1.3 million per year from all respiratory diseases. Although there are several studies on the projected changes in ozone-related health effects under different climate change and demographic scenarios (West et al., 2007; Silva et al., 2016; Turnock et al., 2023; Pozzer et al., 2023; Akritidis et al., 2024), studies on the health effects of ozone during the historical period are lacking. In particular, few studies have quantified the change in risk to human health and the drivers behind this change over this period.

Here, we make use of hourly mean surface ozone concentrations from three CMIP6 models that conducted historical transient experiments – a time resolution that has not been made available in previous global multi-model intercomparison exercises. This has allowed us to calculate an ozone metric relevant to human health (OSDMA8) and explore the simulated changes in concentrations and impacts on human health over the entire CMIP6 historical period (1850 to 2014). In addition, we also use output from sensitivity experiments conducted by one of the CMIP6 models to explore the impact of changes in the different drivers of ozone formation (precursor emissions, stratospheric ozone, aerosols and climate) on the simulated concentrations and how this relates to changes in the risk to human health from long-term exposure to ozone over the same time period.

2 Methods

2.1 CMIP6 model data

We use output from the histSST experiments conducted by three different CMIP6 models as part of the Aerosols and Chemistry Model Intercomparison Project (AerChemMIP), a CMIP6-endorsed Model Intercomparison Project (Collins et al., 2017). The histSST experiments were designed to be an atmosphere-only representation of the coupled historical experiments conducted by individual models using historical forcing data over the period 1850 to 2014. The three models used here, UKESM1-0-LL (Sellar et al., 2019, 2020), GFDL-ESM4 (Horowitz et al., 2020; Dunne et al., 2020) and EC-Earth3-AerChem (van Noije et al., 2021), are all global Earth system models with horizontal grid areas coarser than 100 km. All three models include an interactive representation of chemistry and aerosols, with different couplings and feedback within the Earth system, e.g. land surface and radiation. All models used in this study prescribe long-lived greenhouse gases and methane as global annual concentrations. Table A1 in the Appendix shows a brief description of relevant chemistry and aerosols processes in the three different CMIP6 models. They are, therefore, suitable to use for simulating the long-term responses to surface ozone from perturbations to different drivers of ozone formation, along with any feedback from changes in climate.

Results have been obtained from UKESM1-0-LL for all the other transient historical sensitivity experiments, as this was the only model to complete all of the additional experiments requested, as part of AerChemMIP (Collins et al., 2017), and thus provides hourly surface ozone concentrations. These additional sensitivity experiments involved running the historical transient simulation but with different short-lived climate forcers fixed at pre-industrial values (fol-

lowing an "all-but-one methodology"), including CH_4, NO_x, CO, non-CH_4 VOCs and aerosols. A separate experiment was also conducted to consider the impact of ozone-depleting substances (ODSs – chlorofluorocarbons and hydrochlorofluorocarbons) on stratospheric ozone by fixing their concentrations at 1950 values. An additional experiment to those specified in AerChemMIP was conducted to examine the influence of historical climate change, where the underlying climate conditions (sea surface temperatures and sea ice cover) were kept fixed at 1850 values throughout the whole historical time period. A full list of the experiments analysed here is presented in Table 1.

Hourly mean surface ozone concentrations were obtained from each of the experiments for a single model realisation over the entire historical period (1850–2014). These values were then used to calculate the relevant peak-season ozone health metric (OSDMA8) by first calculating the daily maximum of 8 h running-mean values over a 24 h period, and then a 6-month running mean is calculated from these values. An annual maximum is then calculated to represent the seasonal maximum daily exposure values (avoiding biases from different peak seasons across the world), which is consistent with the metric used in the current WHO air quality guideline values (https://apps.who.int/iris/handle/10665/345329, last access: 30 August 2024). Regional-mean OSDMA8 values have been calculated for the 21 regions used in the GBD study (region definitions shown in Fig. A1).

Surface ozone concentrations are simulated at a relatively coarse resolution (> 100 km) by the CMIP6 models used in this study, which can pose problems when assessing the associated impacts on air quality and human health. Additionally, previous evaluations have shown that global chemistry climate models tend to overestimate surface ozone concentrations (Young et al., 2018; Turnock et al., 2020). To provide a more accurate representation of surface ozone concentrations, which is necessary when linking concentrations to health effects from long-term exposure, the concentrations simulated by each model in the present-day period (2005–2014) have been corrected for biases against the Regionalised Air Quality Model Performance (RAMP) dataset (Becker et al., 2023). The RAMP dataset provides a high-resolution ($0.1° \times 0.1°$) global surface ozone dataset from 1990 to 2017 using state-of-the-art geostatistical methods to integrate surface ozone observations with output from multiple atmospheric chemistry models (including contributions from the GFDL-AM4 model – the atmospheric-model version of GFDL-ESM4). The RAMP dataset directly provides ozone concentrations as OSDMA8 values, which are used to correct the corresponding OSDMA8 values simulated by each CMIP6 model. First, each model is regridded to the finer spatial resolution of the RAMP dataset. We then use OSDMA8 values over the last 10-year mean period (2005–2014) from the RAMP dataset to correct for the absolute difference simulated in the same time period by the CMIP6 models. Using the data from the most recent 10-year mean period (2005–2014) from the historical experiments maximises the availability of ground-based observations in the RAMP dataset used for correction. Figure 1 shows the OSDMA8 values simulated by the 10-year mean (2005 to 2014) in the histSST experiment and the difference compared to the RAMP dataset in the same time period (i.e. the correction applied to each CMIP6 model). EC-Earth3-AerChem shows a consistent overestimation of OSDMA8 concentrations across all regions (up to 20 ppb), whilst GFDL-ESM4 and UKESM1-0-LL have smaller underestimations and overestimations of OSDMA8 values across different regions. Applying this correction to each model for the 2005 to 2014 10-year mean period provides a present-day climatological baseline for each model that can be used as a baseline for long-term changes and also in the calculation of the human health response to exposure, as the simulated concentrations align as much as possible with observations now and the known biases in surface ozone concentrations have been reduced. Staehle et al. (2024) evaluated the performance of four different techniques for bias-correcting surface ozone in global chemistry–climate models. The techniques assessed included mean bias, relative bias, delta correction and quantile mapping. Staehle et al. (2024) recommended using the delta-correction method for correcting future projections of surface ozone due to its lower errors compared to mean and relative bias and its numerical simplicity compared to quantile mapping. Delta correction has also been used as a method in other recent air pollution health studies (Akritidis et al., 2024; Pozzer et al., 2024). Therefore, based on the recommendations of Staehle et al. (2024) and other recent studies, we use the delta-correction method to calculate the change in historical ozone concentrations by applying the ratio of change between each decadal mean and the present day (2005–2014) on top of the bias-corrected baseline for each model. This then generates a new historical time series for each experiment that is connected to the observed present-day values. The temporal changes in OSDMA8 values (from histSST) are calculated by comparing each 10-year mean period to the 2005–2014 baseline period. The contribution of each individual historical driver is obtained through a comparison of different pairs of bias-corrected model experiments, i.e. a control experiment (histSST) compared with an individual sensitivity experiment in which an individual driver is fixed (e.g. piNO_x). The contribution of each individual driver is calculated by taking the difference between OSDMA8 concentrations in the same 10-year mean time period between each of these paired experiments. For example, to quantify the contribution of NO_x emissions to OSDMA8 concentrations in the 2005 to 2014 time period, the 10-year mean OSDMA8 values in this time period from the piNO_x experiment (where NO_x emissions are fixed at 1850 values) are subtracted from the values in the same time period of the histSST experiment (where NO_x emissions have changed), i.e. histSST minus piNO_x. This example quantifies the change in OSDMA8 concentrations in the 2005 to

Table 1. The configuration of the historical sensitivity experiments used in this study. The three CMIP6 models EC-Earth3-AerChem, GFDL-ESM4 and UKESM1-0-LL all provide data for histSST, whereas only UKESM1-0-LL provides data for the other experiments. Methane is prescribed as a global concentration value in these experiments. Aerosol precursors are prescribed global emission datasets of black carbon, organic carbon and sulfur dioxide. Ozone precursors are prescribed global emission datasets of NO_x, CO and non-CH_4 VOCs. Halocarbons are prescribed global concentrations of CFC/HCFC. Climate is represented by prescribed global datasets of sea surface temperatures and sea ice concentrations.

	Anthropogenic air pollutant precursors				
Scenario	Aerosols	Ozone (non-CH_4)	Methane	Halocarbons	Climate
histSST	Transient	Transient	Transient	Transient	Transient
piSST	Transient	Transient	Transient	Transient	Fixed at 1850
1950HC	Transient	Transient	Transient	Fixed at 1950	Transient
piAer	Fixed at 1850	Transient	Transient	Transient	Transient
piCH4	Transient	Transient	Fixed at 1850	Transient	Transient
piO3	Transient	Fixed at 1850	Transient	Transient	Transient
piNOx	Transient	NO_x only fixed at 1850	Transient	Transient	Transient
piVOC	Transient	CO and VOC fixed at 1850	Transient	Transient	Transient

2014 time period from NO_x emissions if they had increased from 1850 to 2014 values. This method is then repeated for each individual driver using the relevant control and sensitivity experiment pairs.

A feature of the histSST sensitivity experiments conducted by UKESM1-0-LL is the use of prescribed values of global CH_4 concentrations, which are unable to respond to any other perturbation of the inputs (e.g. fixing NO_x emissions at 1850 values), in the same way as a CH_4 emission-driven model would. This experimental setup, therefore, neglects the impacts of any of the sensitivity experiments on global CH_4 concentrations and also, consequently, ozone, as CH_4 is a precursor to ozone formation. Therefore, in each of the histSST sensitivity experiments, we have adjusted the ozone concentrations to account for the consequences of changes in the CH_4 lifetime (from the feedback of its own concentrations). Firstly, a global CH_4 lifetime is calculated for each experiment, including histSST. The CH_4 feedback factor (Prather, 1996) is then calculated using the difference in the CH_4 lifetime and CH_4 concentrations between the histSST and histSST-piCH4 experiments over the 30-year period from 1930 to 1960, when large changes in CH_4 concentrations occur but influences from other factors, e.g. halocarbons (Stevenson et al., 2020), are smaller. The CH_4 feedback factor is calculated to be 1.30 over this 30-year period, which is similar to other previous estimates (O'Connor et al., 2021; Stevenson et al., 2013). The feedback factor and CH_4 lifetime can then be used to calculate the equilibrium CH_4 concentrations in each experiment from the transient prescribed values used. The differences in prescribed and equilibrium CH_4 concentrations can be used as input to the relationship between CH_4 perturbations and ozone responses derived by Wild et al. (2012) and subsequently updated by Turnock et al. (2018). This relationship was obtained by analysing the ozone response of multiple chemistry transport models in an experiment where the global CH_4 concentrations were reduced by 20 %, conducted as part of phases 1 and 2 of the Hemispheric Transport of Air Pollutant (HTAP) project. A non-linear relationship is then used to scale this ozone response (calculated from the HTAP 20 % global CH_4 reduction experiment) by the ratio of the global CH_4 abundance change in this study (the difference between equilibrium and prescribed concentrations) relative to the 20 % abundance change used in the original HTAP experiments. From this, we now calculate for each sensitivity experiment the response in surface ozone concentrations that occurs due to the change in CH_4 concentrations resulting from the adjustment in CH_4 lifetime. The model-simulated ozone concentrations are then adjusted accordingly in each of the histSST sensitivity experiments for this change. Four of the sensitivity experiments (piSST, 1950HC, piNOx and piO3) result in increases in CH_4 concentrations and, subsequently, relatively small increases in ozone, whereas, in the other three sensitivity experiments (piAer, piCH4 and piVOC), there are small reductions in CH_4 and ozone concentrations. The magnitude of adjustment to the ozone response slightly varies across regions in each sensitivity experiment, although the sign of change is the same. These ozone values adjusted for the impact of CH_4 lifetime can then be used to calculate the historical changes in surface ozone values relative to the bias-corrected baseline period.

2.2 Emissions in historical scenarios

There have been large changes in emissions of ozone precursors (CO, NO_x, non-CH_4 VOCs and CH_4) since 1850 due to increasing human industrial activity and economic development (Hoesly et al., 2018). Figure 2 shows the relative change (compared to 1850 values) in these ozone precursors, which are used as input to the CMIP6 historical experiments and sensitivity experiments considered in this study (Table 1). Global anthropogenic emissions of NO_x have seen the

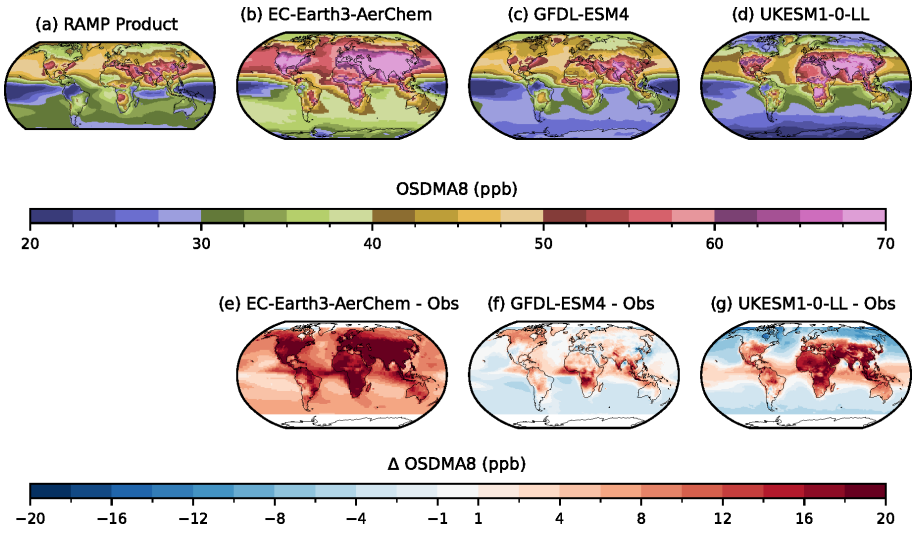

Figure 1. The 10-year mean surface OSDMA8 values (2005 to 2014) from the **(a)** RAMP observational dataset (Becker et al., 2023) and simulated by three CMIP6 models: **(b)** EC-Earth3-AerChem, **(c)** GFDL-ESM4 and **(d)** UKESM1-0-LL, and the differences for the same models **(e–g)** when compared to the RAMP observational dataset (Becker et al., 2023) over the same time period.

largest increase in the ozone precursor emissions: a fractional increase of > 10 globally since 1850. Global emissions of non-CH_4 VOCs and CO, along with global CH_4 concentrations, have increased globally by a fractional change of > 1 (i.e. more than doubled) since 1850. These large changes will all have a substantial effect on surface ozone concentrations throughout the historical period considered in the CMIP6 experiments (1850 to 2014). Additionally, changes in climate and stratospheric ozone concentrations over the historical period will also have an influence on surface ozone concentrations; the changes in these are considered in the sensitivity experiments in Table 1. The transient change in surface air temperature simulated by UKESM1-0-LL over the historical period (Fig. 2 right panel) showed particularly large cold biases compared to observations throughout the latter half of the 20th century (peak of ≈ 0.5 K), which were similar to a number of other CMIP6 models (Flynn and Mauritsen, 2020). The cold-temperature biases simulated by UKESM1-0-LL have been previously attributed to an excessive aerosol forcing, with recent changes to aerosol and cloud properties in an updated version (UKESM1-1-LL) showing an improved representation of historical surface temperatures (Zhang et al., 2021; Mulcahy et al., 2023). However, in 2014, the global annual mean surface temperature in both HadCRUT5 observations (Morice et al., 2021) and UKESM1-0-LL simulations (Fig. 2) increased by a similar amount of $\approx$ 1 K (compared to an 1850 to 1900 mean period), mainly due to increasing concentrations of long-lived greenhouse gases (Chen et al., 2021). Total-column ozone burdens have shown large reductions since the 1960s in UKESM1-0-LL historical simulations due to the reductions in stratospheric ozone from increases in ozone-depleting substances, e.g. CFCs. However, total-column ozone simulated by UKESM1-0-LL in CMIP6 simulations tends to be higher than other CMIP6 models and observations and also simulates a stronger depletion of stratospheric ozone from 1960 to 2000 (Keeble et al., 2021). All of these drivers of surface ozone are used as transient changes to the inputs for the histSST experiment and are also fixed at 1850 values (or 1950 for ODS) for the individual sensitivity experiments.

2.3 Health calculations

To assess the health impacts from long-term exposure to ozone concentrations during the historical period, we use the attributable fraction (AF) metric, which is defined here as the percentage of deaths from chronic obstructive pulmonary disease (COPD) attributable to ozone pollution. A full health assessment is not undertaken due to the absence of long-term datasets for changes in population (on a latitude–longitude grid) and country-specific baseline mortality rates over the 1850 to 2014 period. In more detail, $\mathrm{AF}(x, y, t)$ is calculated at a given location with x and y coordinates and for a specific time period t, as shown in Eq. (1):

$$\mathrm{AF}(x, y, t) = \frac{\mathrm{RR}(x, y, t) - 1}{\mathrm{RR}(x, y, t)}, \tag{1}$$

where $\mathrm{RR}(x, y, t)$ is the relative risk (also known as hazard ratio) for ozone-related excess mortality from COPD. Following the GBD 2019 methodology (Murray et al., 2020), RR is estimated using a log-linear function, as shown in Eq. (2):

$$\mathrm{RR}(x, y, t) = e^{\beta(X(x,y,t) - \mathrm{TMREL})}, \tag{2}$$

where $X(x, y, t)$ is the health-relevant ozone metric (OSDMA8) at the given location and time period, and TMREL

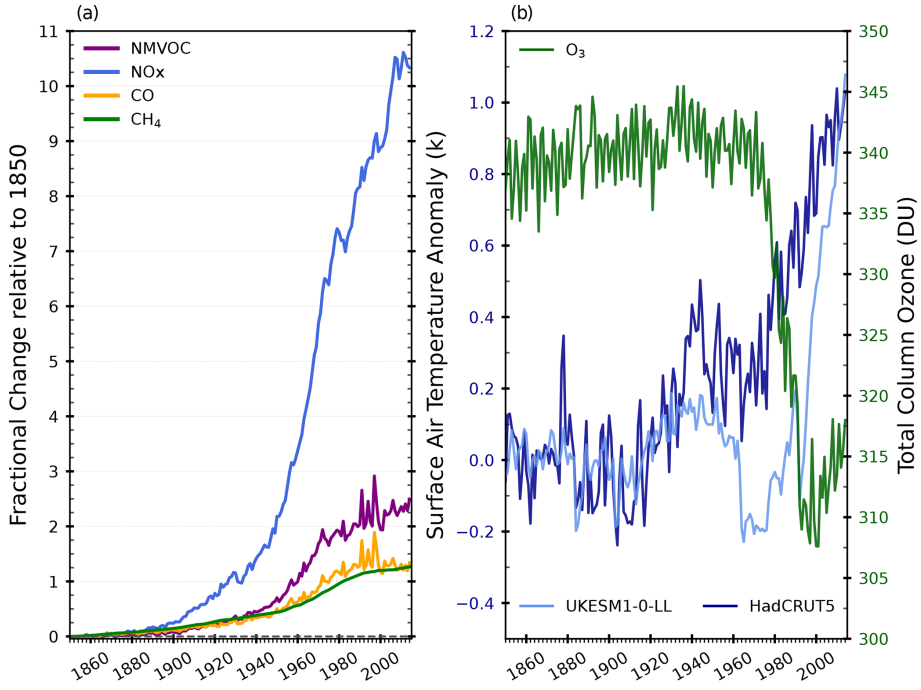

Figure 2. Relative change in total historical emissions of ozone precursors (NO_x, CO and NM(non-CH_4) VOCs) and global CH_4 concentrations compared to 1850 values **(a)**. Global annual mean surface air temperature anomaly, relative to an 1850–1900 mean period, from UKESM1-0-LL historical simulations and HadCRUT5 (Morice et al., 2021) (blue lines, **b**). Global annual mean total-column ozone values from 1850 to 2014 simulated by UKESM1-0-LL (green line, **b**).

is the theoretical minimum risk exposure level, below which ozone is considered as not being harmful for human health. For TMREL, we adopted the value of 32.4 (29.1–35.7) ppb, while the β parameter value or values can result from the RR per 10 ppb of ozone (OSDMA8) value of 1.063 (1.029–1.098), estimated from a meta-regression of five cohort studies (Murray et al., 2020).

Since ozone concentrations (OSDMA8) are the only varying input in the AF calculations, the AF temporal changes over the historical period reflect the changes in the percentage of ozone-related COPD excess mortality from ozone variations only. The ozone exposure values were calculated as 10-year mean OSDMA8 values across the historical period from the bias-corrected model simulation data. An assessment of population exposure to ozone is also provided by calculating the number of people exposed to OSDMA8 concentrations above the TMREL in three different decadal time periods (1850–1859, 1980–1889 and 2005–2014). Population data for these periods are obtained for the nearest available years (1850, 1980 and 2010) from the Hyde dataset (History database of the Global Environment) (Klein Goldewijk et al., 2017).

Attribution of ozone health effects (AF) to different drivers by taking the difference between the reference and sensitivity simulations is not valid, as AF is not directly proportional to OSDMA8 concentrations but rather depends on whether ozone exceeds the TMREL and by how much. This type of decomposition would be feasible if the actual percentage contribution of each driver to the total OSDMA8 change could be estimated, which is not possible in the current approach due to the non-linearities in ozone chemistry. Therefore, only qualitative insights can be made on the relative contributions of each driver to ozone health effects. Thus, AF in a sensitivity simulation should be viewed as a conceptual indicator, reflecting the potential health impacts under a specific scenario (e.g. pre-industrial NO_x emissions in near-present-day conditions), without providing a direct attribution of the health effects of ozone to individual drivers in the real-world context.

3 Results

3.1 Multi-model historical changes in surface ozone and risk to human health

3.1.1 Multi-model historical changes in OSDMA8

The regional-mean change in OSDMA8 concentrations over the 1850 to 2014 period from the three bias-corrected CMIP6 models is shown in Fig. 3. Large changes in OSDMA8 concentrations have been simulated across all regions over the historical period. Globally, the 10-year multi-model mean ($\pm$1 SD of three model values) OSDMA8 concentrations are simulated to have increased by 12 ± 2.6 ppb (50 % increase) between 10-year mean values centred on 1855 and 2010,

which is of similar magnitude to annual mean changes simulated by six CMIP6 models (Turnock et al., 2020) and other previous global chemistry–climate-model intercomparison studies (Young et al., 2013). In addition, this simulated historical change in global OSDMA8 is within the observed changes in surface ozone across the Northern Hemisphere from 30 % to 70 % (approximately 10 to 16 ppb) from Tarasick et al. (2019). The largest regional-mean increases over the same time period have been simulated to occur over South Asia (29.8±5.3 ppb, 115 %), East Asia (24.8±2.2 ppb, 88 %), high-income Asia Pacific (24.8 ± 0.4 ppb, 110 %), North Africa and the Middle East (21.4±4.8 ppb, 78 %), central Europe (21.3 ± 3.9 ppb, 90 %), and high-income North America (18.6 ± 1.9, 81 %). Previously, CMIP6 models were shown to be able to represent the multi-decadal changes in surface ozone concentrations since 1960 at five remote long-term monitoring locations around the world (Griffiths et al., 2021). Even though this comparison is spatially limited, due to the availability of monitoring locations with multi-decadal observational records, it does provide a degree of confidence in the ability of models to simulate long-term changes at specific remote locations, representative of background conditions. Across most regions, OSDMA8 concentrations only show small increases up until about 1950. After this time period, concentrations rapidly increase (by approximately 50 %) to 2005–2014 values, driven by the large rapid changes in all anthropogenic precursors of ozone (CH_4, NO_x, CO and non-CH_4 VOCs), with the largest relative changes occurring in NO_x emissions (Fig. 2). The increase in concentrations continued across certain regions, most notably South Asia, East Asia, and other tropical and sub-tropical regions due to the continued increases in anthropogenic ozone precursors from socio-economic development across these regions (Fig. A3). However, across some regions in the northern mid-latitudes (high-income North America, Europe and high-income Asia Pacific) OSDMA8 concentrations stopped increasing from about the 1980s, remaining at and near these values until the end of the CMIP6 historical period when a slight reduction in concentrations occurred, in agreement with the observations in the RAMP dataset (Fig. 3). The recent change in OSDMA8 concentrations is consistent with mitigation measures adopted in these regions to improve regional air quality by reducing primary air pollutant emissions (United Nations Economic Commission for Europe, 2004; EMEP Steering Body and Working Group on Effects of the Convention on Long-Range Transboundary Air Pollution, 2016), shown by a reduction in NO_x emissions from the peak in the 1980–1990s (Fig. A3).

Figure 3 shows that bias-correcting the model data to the RAMP dataset has resulted in the simulated OSDMA8 concentrations from all three models being similar in the 2005 to 2014 10-year mean period. However, there is still a diversity of 10 % to 15 % in the model simulated OSDMA8 concentrations from the pre-industrial period (1850 to 1860), with one of the largest model differences (20 %) occurring over South Asia. UKESM1-0-LL consistently simulates larger bias-corrected OSDMA8 concentrations across most regions in the first 10-year mean period of 1855, with GFDL-ESM4 tending to have the lowest concentrations of the three models. This diversity between models can be attributed to differences in how they represent chemical processes (see Table A1); particularly relevant to the pre-industrial period are differences in the representation of meteorology/climate as well as interactive/natural components such as emissions from biogenic sources (BVOCs), lightning NO_x and wetland CH_4 (Rowlinson et al., 2020; Wild et al., 2020). In addition, differences in resolution (both horizontal and vertical) and chemical mechanisms between each of the models can also contribute to the highlighted diversity in simulated ozone concentrations (Wild and Prather, 2006; Wild et al., 2020). These structural differences between models also impact the chemical sensitivity of ozone formation in each model, resulting in the different simulated historical changes in OSDMA8 across the models (Turnock et al., 2020). Given its higher 1855 concentrations, UKESM1-0-LL is the model that tends to simulate the smallest historical change in OSDMA8 values over the historical period (9.2 ppb globally), whilst GFDL-ESM4 simulates the largest (14.3 ppb globally). If the models are not corrected against the observation-based dataset, then the simulated concentrations show on average a larger (20 %) variability between models (up to 30 % across South Asia), with the largest diversity in concentrations in the 1855 period. The comparison to the RAMP dataset in the 2005 to 2014 period shows that simulated OSDMA8 values tend to be consistently overestimated by all three models (Figs. 1 and A2). Overestimating OSDMA8 concentrations has important consequences for the assessment of the long-term impact on human health due to the use of theoretical minimum risk exposure level, below which no risk to health is considered (Sect. 2.3). Using the uncorrected simulated OSDMA8 concentrations from the models could result in an overestimation of the impacts on human health from long-term exposure, and thus the bias-corrected model simulated concentrations are used for any assessment of health impacts.

3.1.2 Historical changes in ozone exposure and risk to human health

The increase in OSDMA8 concentrations over the historical period across all regions has increased the risk to human health via enhanced long-term exposure to ozone. Figure 3 shows how the simulated regional OSDMA8 concentrations compare with the TMREL of 32.4 ppb. All three models simulate concentrations in the first 10-year mean period of 1855 that are below this threshold across most regions of the world, resulting in < 20 % of the world's population in 1850 being exposed to concentrations above this value (Fig. 4a). However, the simulated increase in OSDMA8 concentrations over the historical period has resulted in con-

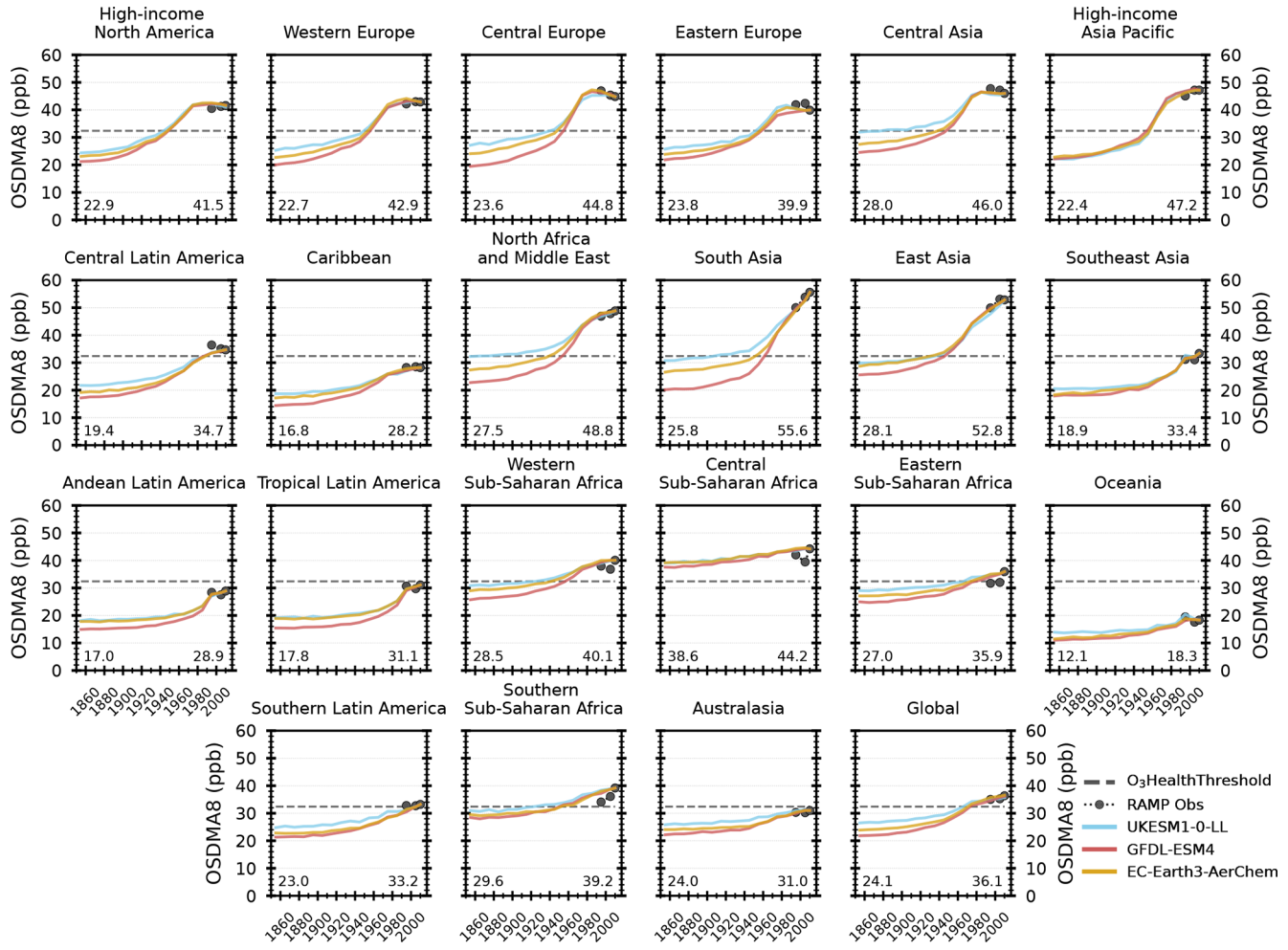

Figure 3. Regional-mean surface OSDMA8 values from three CMIP6 models simulated over the historical period (1850–2014) bias-corrected to a 10-year mean of observations from Becker et al. (2023). Observations from Becker et al. (2023) are shown as circles on each relevant region with the TMREL value of 32.4 ppb as the dashed line. Regional multi-model mean OSDMA8 values are shown for the start and end of the time period.

centrations being above the TMREL value in almost every region of the world in the near-present-day period. This is shown by $> 90\,\%$ of the world's population in 2010 being exposed to ozone concentrations above this value, meaning that over the historical period there has been a large increase in the risk to human health from long-term exposure to elevated ozone concentrations.

Figure 5 shows the spatial distributions of the multi-model mean attributable fraction over the pre-industrial period (1850–1859) and the near-present-day period (2005–2014). High-AF values up to $\approx 20\,\%$ are found over regions of northern India, eastern China, the Middle East, and the western United States, indicating that across these regions approximately one out of five COPD deaths in the near-present-day period is attributed to long-term ozone exposure. High-AF values of $> 8\,\%$ also occur over Greenland in 2005–2014, which can be attributed to the presence of the high-altitude ice sheet (≈ 2000 m a.s.l. – above sea level), meaning that the ozone concentrations are not representative of typical surface values for this latitude but can be considered more like elevated free-tropospheric ozone concentrations. As the AF calculation does not consider changes in population and baseline mortality rates, a distinct increase in the AF is depicted almost globally compared to the 1850–1859 period due entirely to increases in ozone concentrations. As ozone concentrations in the pre-industrial period are below the TMREL value almost all over the world, the respective AF values are near zero. The major exception to this is that AF values are approximately $5\,\%$ in the 1850–1859 period over the central Sub-Saharan Africa region. This non-zero AF is due to the elevated pre-industrial OSDMA8 concentrations (Fig. 3) arising mainly from biomass burning sources of ozone precursors over this region in this period, although the low population density in this region and

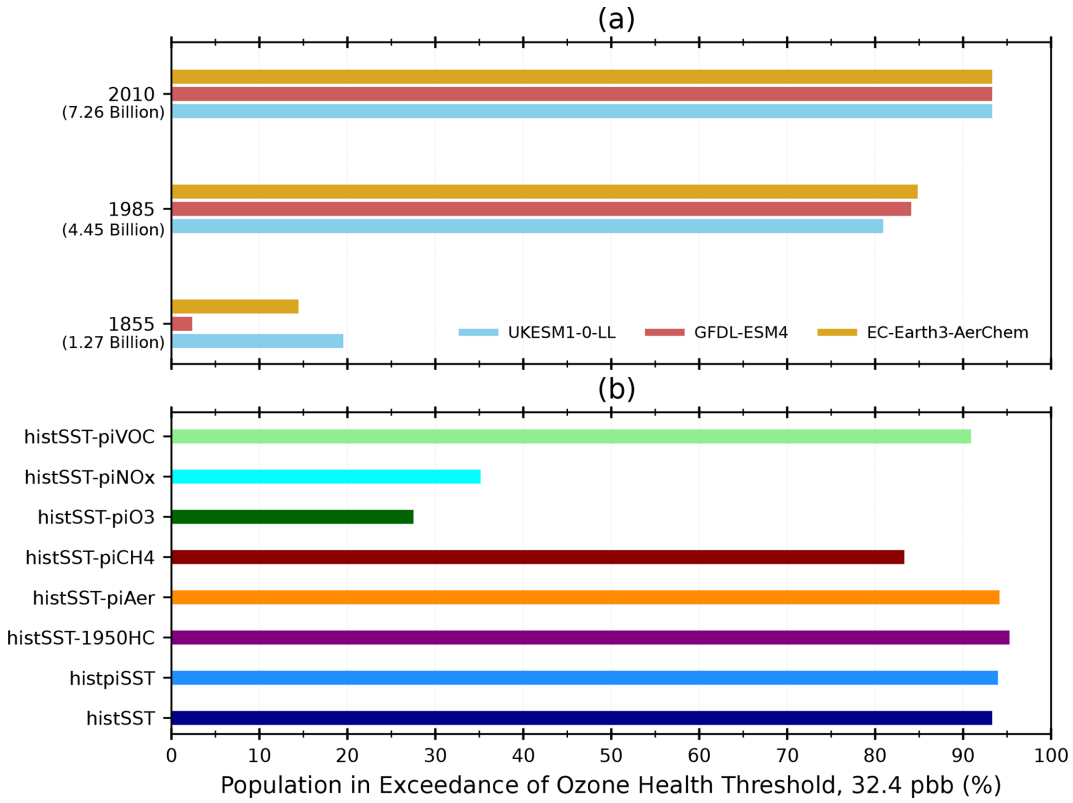

Figure 4. Percentage of total global population in exceedance of the theoretical minimum risk exposure level (TMREL – 32.4 ppb) for ozone across three historical time periods, from three different CMIP6 models **(a)** and for the present day (2010) under sensitivity scenarios with different drivers of ozone fixed **(b)**. Total global population for each time period is shown in parenthesis on **(a)**.

time period would represent a low risk to health. Overall, this suggests that there is no risk for human health from ozone exposure in the pre-industrial period, although the increases in ozone concentrations up to the near-present-day became a major threat for human health, being responsible for more than 10 % of COPD deaths in many regions of the Northern Hemisphere.

3.2 Drivers of historical change in surface ozone and risk to human health

3.2.1 Drivers of historical change in OSDMA8 concentrations

Figure 6 shows the change in OSDMA8 concentrations in the present-day period (2005 to 2014) due to the historical changes in all drivers together (histSST) and due to the individual drivers of ozone formation, i.e. histSST minus sensitivity experiment. The overall change in global mean OSDMA8 concentrations simulated by UKESM1-0-LL over the historical period in histSST is 9.2 ppb. Considering only historical changes in emissions of ozone precursors (i.e. histSST minus histSST-piO3 = NO_x, CO and non-CH_4 VOCs) has resulted in a large increase in global mean OSDMA8 concentrations of 9.6 ppb (37 %) in the 2005 to 2014 mean pe-

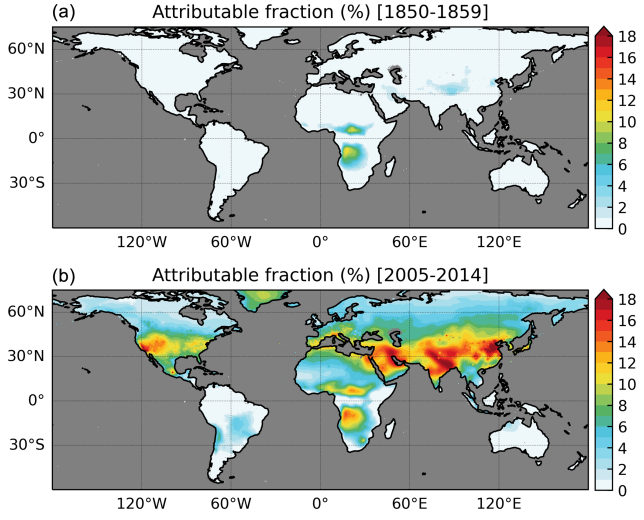

Figure 5. Attributable fraction, as the percentage of deaths from COPD attributable to ozone pollution, calculated from the multi-model mean OSDMA8 values in the 10-year mean periods of 1850–1859 **(a)** and 2005–2014 **(b)**.

riod. Of these three precursors, the majority of this change in global mean OSDMA8 concentrations in 2005–2014 can be attributed to historical changes in anthropogenic NO_x emissions (8.6 ppb, 32 %), compared to CO and non-CH_4 VOCs (1.5 ppb, 4 %). Regionally, the largest changes in OSDMA8 concentrations occur mainly over the polluted continental regions in the northern mid-latitudes. OSDMA8 concentrations increased by ≈25 ppb over the high-income Asia Pacific region, due to this region having the largest relative increase in anthropogenic NO_x emissions over the historical period (Fig. A3). Similarly large increases in OSDMA8 concentrations occur over Europe (16 ppb), high-income North America (16 ppb), East Asia (23 ppb) and South Asia (24 ppb) all mainly due to the large historical changes in anthropogenic NO_x emissions over these regions (Fig. A3). Changes in anthropogenic emissions of ozone precursors, particularly over recent decades, have also been shown, as in this study, to be the most important driver behind changes in regional surface ozone concentrations (Parrish et al., 2014; Zhang et al., 2016; Lin et al., 2017; Yan et al., 2018; Wang et al., 2022).

Historically, global CH_4 concentrations, the other major precursor for gas to ozone formation, have more than doubled since 1850 (Fig. 2), which increased global mean OSDMA8 concentrations by 5.9 ppb (20 %) in the 2005 to 2014 period. The impact of changes in CH_4 on surface ozone concentrations tends to be larger, in emissions and abundance, than other non-methane VOCs and more globally uniform due to its larger change over the historical period, the longer chemical lifetime of CH_4, its larger abundance in the atmosphere and that it is input to these model experiments as a global annual mean concentration rather than gridded emissions. This means the impact of changes in CH_4 on surface ozone in this study is spatially limited by the absence of a hemispheric gradient in CH_4 concentrations (higher in the Northern Hemisphere and lower in the Southern Hemisphere) – something that would be provided if using a model with a fully interactive CH_4 cycle, including CH_4 emissions instead of concentrations (Folberth et al., 2022). The largest increase in OSDMA8 concentrations occurred over parts of Asia, North Africa and the Middle East (up to 8.5 ppb, 21 %), whilst the smallest increase (2 to 3 ppb, 10 % to 13 %) occurred over tropical regions of the Southern Hemisphere. Over some of these more remote (low NO_x) regions like Sub-Saharan Africa and southern Latin America, historical changes in CH_4 had a larger proportional impact on OSDMA8 concentrations, contributing almost as much as changes in NO_x emissions. This shows historical changes in CH_4 concentrations have been important in altering the background ozone concentrations in most regions of the world.

The other drivers of surface ozone formation considered here in the sensitivity experiments are historical changes in climate, aerosols and stratospheric ozone via ODS, which have all tended to have smaller impacts than anthropogenic ozone precursor emissions (see Figs. 6 and A4 for more detail). The increasing emissions of ODS since the 1950s reduced stratospheric ozone concentrations (shown as total-ozone column in Fig. 2) significantly by the start of the 21st century, which has also led to reductions in OSDMA8 concentrations, potentially via less downward transport to the surface or from changes to photolysis rates. Global mean OSDMA8 concentrations were reduced by −2.8 ppb (−7 %) in the 10-year mean period of 2005 to 2014 due to smaller amounts of stratospheric ozone resulting from the increased ODS in the histSST experiment compared to the 1950HC experiment in this most recent period. Some of the largest impacts (> −2 ppb) occurred over remote Southern Hemisphere regions, including southern Latin America and Australasia (Fig. A4). In addition, changes in stratospheric ozone also reduced OSDMA8 concentrations across the well-known hot-spot regions of stratosphere–troposphere transport (STT) (Škerlak et al., 2014; Akritidis et al., 2021) of high-altitude central Asia, the eastern Mediterranean and the Middle East, and the western United States.

Increasing emissions of aerosols and aerosol precursors over the historical period (Fig. A5) has resulted in a small reduction in global mean OSDMA8 concentrations of −0.8 ppb (−2 %) in the 2005 to 2014 period (see Fig. A4 for more detail). Increasing aerosols over the historical period implies there is an increase in the heterogeneous loss of nitrogen oxides to aerosol surfaces (the only active heterogeneous tropospheric mechanism currently in UKESM1-0-LL; Archibald et al., 2020b), leading to a reduction in ozone formation. This effect is probably underestimated due to the absence of the loss mechanism involving HO_2 uptake on aerosols in UKESM1-0-LL (Ivatt et al., 2022). Regionally, increasing aerosols causes the largest reduction in OSDMA8 concentrations of up to −2.1 ppb (−4 %) across Asia (Central, South and East), North Africa and the Middle East regions in the 2005 to 2014 period when aerosol concentrations were higher. However, the largest reduction of OSDMA8 concentrations from aerosols (−2.7 ppb, −6 %) occurred in the 1980s across Europe. Aerosol concentrations peaked in Europe at this time due to the subsequent enacting of air pollutant controls, meaning aerosol concentrations and their impact on surface ozone were reduced thereafter (Turnock et al., 2015).

The climate change signal over the historical period has resulted in an approximate 1K increase in global mean surface temperatures simulated by UKESM1-0-LL over the 2005 to 2014 period (Fig. 2), which has resulted in a small reduction in global mean OSDMA8 concentrations of −0.8 ppb (−2 %) that is consistent with the surface ozone temperature sensitivity of −0.79 ppbv $°C^{-1}$ from Zanis et al. (2022). The global mean reduction in ozone has mainly been driven by decreases over the ocean, which can be attributed to more ozone destruction due to increased hydroxyl formation from enhanced amounts of water vapour occurring in a warmer world (Johnson et al., 1999; Doherty et al., 2013; Zanis et al., 2022). Historical climate change has resulted in enhanced ozone formation rates over some polluted continen-

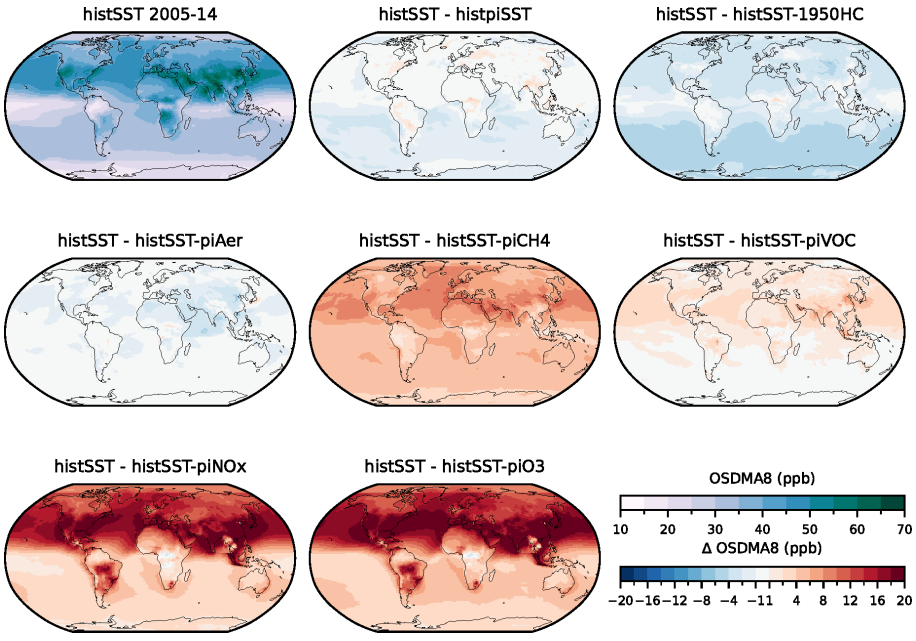

Figure 6. The 10-year mean surface OSDMA8 values simulated by UKESM1-0-LL in the HistSST experiment for 2005–2014 (bias-corrected) and the change in the same time period in the HistSST experiment relative to each sensitivity experiment with different drivers of ozone fixed.

tal regions including South-east Asia, Central Europe, East Asia, high-income Asia Pacific and parts of North America (see Fig. A4 for more detail), which are shown by small increases in OSDMA8 concentrations (< 1 ppb, 2 %). There have also been similar small increases in OSDMA8 concentrations across some major biogenic-emission regions (central Sub-Saharan Africa and parts of South America). This suggests a small climate impact on natural sources of ozone precursor emissions is simulated by the interactive BVOC emission scheme included within UKESM1-0-LL. The magnitude of the changes in ozone due to 1 K of warming over the historical period is consistent with studies analysing the change in ozone in response to future warming (Archibald et al., 2020c; Zanis et al., 2022), with the impact of climate change on surface ozone being less in this study due to the lower level of historical warming compared to projections of future warming of 2.7 to 5.4 K. In addition, Zanis et al. (2022) showed that UKESM1-0-LL had a lower ozone sensitivity per unit temperature change on a global-mean basis (-0.79 ppbv $°C^{-1}$) than other CMIP6 models (multi-model mean of -0.93 ppbv $°C^{-1}$), which could mean that climate change impacts on surface ozone are underestimated in this study. However, this global sensitivity number obscures the spatial variation in the sensitivity of surface ozone to temperature (both positive and negative) across different models (Zanis et al., 2022). The model diversity highlights the facts that the surface ozone response to climate change is still uncertain in global chemistry–climate models and that both stronger and weaker responses are possible across different regions.

In summary, the model experiments isolating the impact of the individual drivers show that historical changes in anthropogenic NO_x emissions contribute the most, approximately 42 %, to the summed total change in historical global mean OSDMA8 concentrations from all drivers combined. The contributions to historical changes in global mean OSDMA8 concentrations from other drivers were 29 % from global CH_4 concentrations, 14 % from stratospheric ozone, 7 % from anthropogenic emissions of CO and non-CH_4 VOCs, and 4 % from both aerosols and climate change. This attribution of drivers is in agreement with other studies that showed reductions in peak-season surface ozone over North America and Europe and increases over East and South Asia between 1980 and 2010 were primarily driven by changes in anthropogenic ozone precursor emissions, with much smaller contribution from other factors including changes in CH_4 concentrations and climate (Zhang et al., 2016; Yan et al., 2018; Wang et al., 2022). However, the linear combination of the historical change in global mean OSDMA8 concentrations, calculated from the individual driver experiments by UKESM1-0-LL ($+11.6$ ppb), is found to be about 20 % larger than that calculated when all drivers are varied simultaneously ($+9.2$ ppb from histSST). At a global scale, this indicates feedback and interactions (e.g. clouds or aerosols influencing photolysis rates) influencing ozone formation in each of the individual experiments due to the changes from that particular driver (Gao et al., 2020; Qu et al., 2021). The

feedback/interactions then have a non-linear effect on the formation of ozone, reducing the magnitude of change in OSDMA8 at the global scale when the drivers are changed in combination with single experiments (histSST). At the global scale, the impact on ozone concentrations due to each individual driver can be considered overestimated, as the change in the combined driver experiment (histSST) is smaller than those from the linear addition of the individual driver experiments.

3.2.2 Drivers of change in ozone exposure and risk to human health

The change in the individual drivers of ozone formation shows different impacts of OSDMA8 concentrations over the historical period, which will also have an impact on the risk to human health via changes to long-term exposure. Figure 4b shows a comparison of the different fractions of the global population in 2010 that are exposed to OSDMA8 concentrations above the TMREL of 32.4 ppb in each of the sensitivity scenarios that isolate the different drivers of ozone formation. If emissions of ozone precursors (NO_x, CO and non-CH_4 VOCs) are kept fixed at 1850 values, then the fraction of the near-present-day global population exposed to OSDMA8 concentrations above 32.4 ppb is substantially reduced to 27 %, down from > 90 % when emissions are allowed to increase in histSST. Fixing solely anthropogenic NO_x emissions at 1850 is shown to be the dominant cause of this reduction by decreasing the global population exposure above the TMREL to 34 %. Fixing the emissions of the other precursors (CO and non-CH_4 VOCs) at 1850 values results in a very small (2 %) change in global population exposure. A relatively small impact on global population exposure is shown when fixing global CH_4 concentrations at 1850, which reduces the proportion of the global population exposed to OSDMA8 concentrations above TMREL to 83 % (from > 90 %). Fixing the other historical drivers of ozone concentrations (climate change, stratospheric ozone and aerosols) slightly increases the global population exposure to OSDMA8 concentrations above the TMREL by 1 % to 2 %. These results show that historical changes in anthropogenic NO_x emissions are the leading cause of increased ozone exposure that is considered harmful to human health.

Figure 7 presents the global and regional-mean AFs for the histSST and sensitivity experiments isolating the different drivers of ozone formation in the near-present-day period (2005–2014). A high health risk from COPD attributable to ozone pollution (histSST) is found in South Asia and East Asia with regional average AFs of 13 % and 12 %, respectively, while values in other regions are North Africa and the Middle East (9 %), high-income Asia Pacific (9 %), Central Europe (7 %), western Europe (6 %), and high-income North America (5 %). Regarding the drivers of ozone changes, fixing NO_x emissions to pre-industrial levels (histSST-piNOx) eliminates the risk for human health from ozone exposure for the 2005–2014 period in most regions. Historical increases in methane concentrations also appear to imply a risk for human health in the near-present-day period both globally and regionally, as setting methane concentrations to pre-industrial levels results in a lower risk for health in the highly populated regions of South Asia, East Asia and western Europe with AF values of 9 %, 7 % and 2 %, respectively. Historical changes in climate, aerosol precursor emissions and stratospheric ozone have relatively small impacts on historical OSDMA8 changes and, consequently, on regional-mean near-present-day AF. Isolating these drivers at 1850 levels (or 1950 for stratospheric ozone) shows only small changes in AF values and therefore in ozone-related health risk.

4 Conclusions

Surface ozone is an important greenhouse gas and secondary pollutant in the lower atmosphere, influencing both the Earth's climate and air quality. Exposure to elevated concentrations of ozone at the surface can have detrimental impacts on human health. In this work, we use numerical results of hourly surface ozone, obtained from the latest generation of global chemistry–climate models that participated in CMIP6 as part of the Aerosol and Chemistry Model Intercomparison Project (AerChemMIP). For the first time, we use hourly surface ozone output from three different CMIP6 models, over the 165-year historical period (1850 to 2014), to calculate changes in the peak-season ozone metric (OSDMA8), which can relate risks to human health from long-term exposure surface ozone. All three CMIP6 models tended to overestimate the recently observed OSDMA8 concentrations, in agreement with other recent multi-model evaluations of surface ozone concentrations (Young et al., 2018; Turnock et al., 2020). The data from the most recent 10-year mean period (2005 to 2014) of OSDMA8 concentrations simulated by the three CMIP6 models were bias-corrected to the observations to avoid overestimating the present-day risk to human health from long-term ozone exposure. However, there is still a 10 % to 15 % difference in the simulated OSDMA8 concentrations in the pre-industrial period (1850 to 1859) due to physical and chemical differences across the three models, which also influences the magnitude of the simulated historical change in OSDMA8. Global increases of more than 50 % in OSDMA8 concentrations were simulated over the historical period by all three CMIP6 models, with the largest changes over the Northern Hemisphere regions (North America, Europe and Asia). This change has increased the proportion of the global population being exposed to OSDMA8 concentrations above the theoretical minimum risk exposure level (TMREL), below which ozone is considered as not being harmful for human health, from less than 20 % in 1855 to more than 90 % in 2010. The risk to human health from long-term exposure to ozone concentrations has been assessed in terms of changes to the attributable

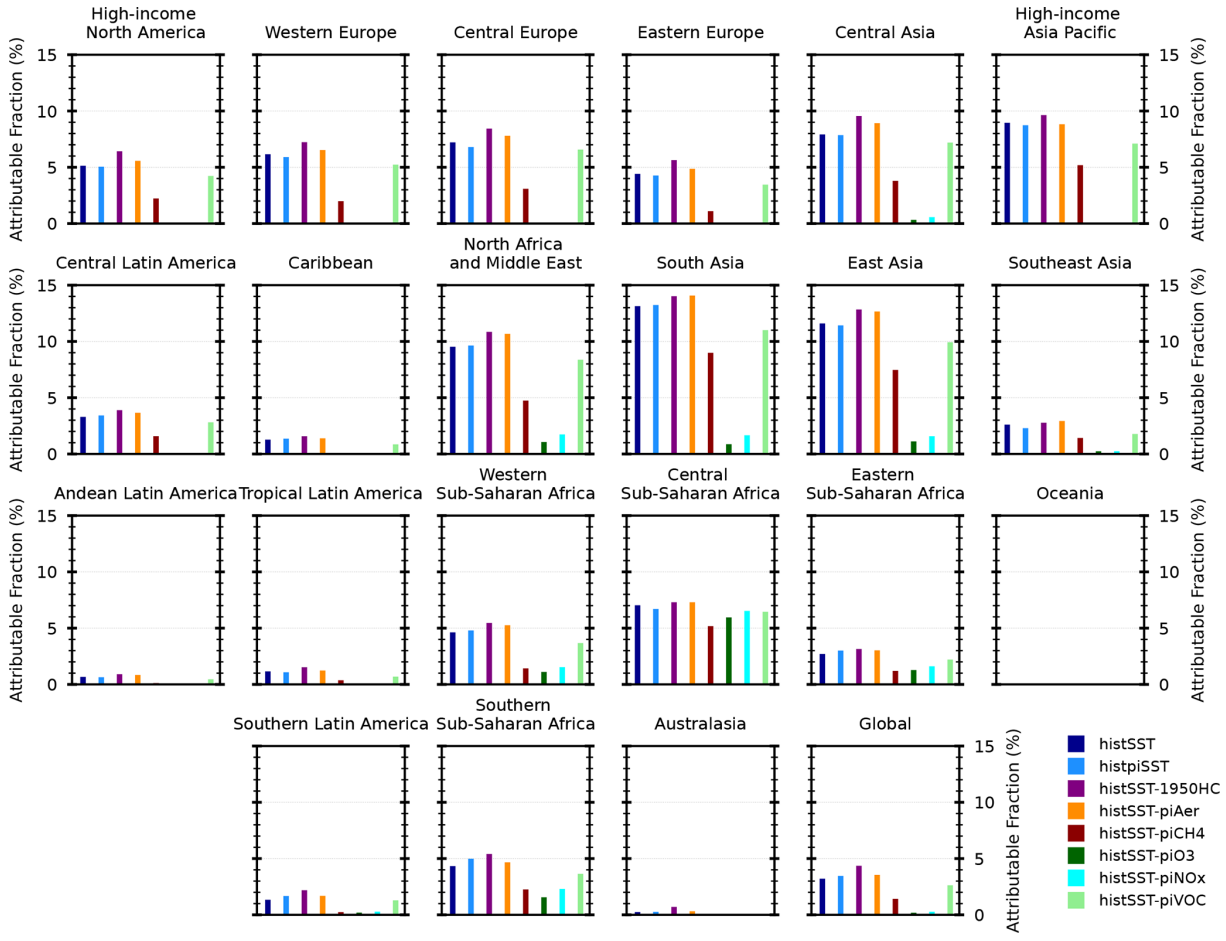

Figure 7. Regional-mean attributable fraction as the percentage of deaths from COPD calculated from the 10-year (2005–2014) mean OSDMA8 values simulated by UKESM1-0-LL in the HistSST and sensitivity experiments with different drivers of ozone fixed.

fraction (AF), defined here as the percentage of deaths from chronic obstructive pulmonary disease (COPD) attributable to ozone pollution. The AF has increased by more than 10 % over many regions of the Northern Hemisphere, showing that increased ozone concentrations over the historical period have contributed to a significant increase in the long-term risk to human health across many populated regions of the world. In addition, the historical increase in surface ozone concentrations has made the risk of human mortality from long-term exposure to ozone similar to other environmental risk factors, but the risk is still much less than from long-term exposure to fine particulate matter (GBD 2021 Risk Factors Collaborators, 2024).

An analysis of the drivers of historical changes in OSDMA8 concentrations and risks to human health is provided from hourly surface ozone outputs of sensitivity experiments conducted using a single CMIP6 model that isolates the historical changes in ozone precursors (NO_x, CO, non-CH_4 VOCs and CH_4), anthropogenic aerosols, ozone-depleting substances and climate change. Historical increases in anthropogenic emissions of NO_x are identified as the leading contributor to increases in OSDMA8 concentrations (≈ 40 % globally) over the period from 1850 to 2014, particularly over Northern Hemisphere regions. Increases in global CH_4 concentrations are also shown to have an important contribution to historical changes in OSDMA8 concentrations (≈ 30 % globally), particularly over more Southern Hemisphere regions, where its contribution can be as large as that from NO_x. The increase in anthropogenic emissions of other ozone precursors (CO and non-CH_4 VOCs) has had a relatively small impact on increasing historical OSDMA8 concentrations (≈ 7 % globally) compared to NO_x and CH_4. The other drivers considered here (stratospheric ozone, aerosols and climate change) all have relatively small contributions to historical changes in OSDMA8 concentrations. The depletion of stratospheric ozone since the 1950s has resulted in less downward transport of ozone to the surface and a small reduction in historical surface concentrations, particularly over more remote Southern Hemisphere regions. Increasing anthropogenic emissions of aerosols also caused a small reduction in OSDMA8 concentrations, particularly over Asia, although this effect might be underes-

timated due to an under representation of heterogeneous-chemistry mechanisms within the model (Ivatt et al., 2022). Historical climate change contributed to small reductions in historical OSDMA8 concentrations over remote regions and a small increase over polluted continental regions due to changes in ozone production and destruction pathways. The response of ozone to climate change was small due to the small 1K of global warming considered over the historical period, although the results were consistent with projected changes due to future warming (Zanis et al., 2022).

Increasing anthropogenic NO_x emissions over the 1850 to 2014 period is shown to be the main contributor to the long-term health effects from ozone exposure in the near-present-day period (2010). Fixing anthropogenic NO_x emissions at 1850 reduces the proportion of the near-present-day global population exposed to OSDMA8 concentrations above the TMREL to 34 %, from more than 90 % when they are allowed to increase over the historical period along with other precursors. Fixing NO_x emissions at 1850 also reduces the AF to near zero across most regions, thereby eliminating the risk to human health from long-term ozone exposure. Historical global CH_4 concentrations are shown to be the next most important contributor to the health effects from long-term ozone exposure. Fixing global CH_4 concentrations at 1850 values reduces the proportion of the global population exposed to OSDMA8 concentrations above the TMREL to 83 %, reduces the AF and reduces the risk to human health by about half in populated regions. However, the influence of the other drivers is small, having little impact on the health risk of the near-present-day population from exposure to elevated surface ozone concentrations.

The results from these experiments provide a unique opportunity to quantify the long-term changes, and attribution to multiple drivers behind the changes, of an ozone exposure metric relevant to health impacts over a 165-year period from 1850 to 2014. Substantial increases have occurred in surface ozone concentrations and the risk to human health from long-term exposure to these elevated concentrations over the historical period. These changes can be mainly attributed to changes in anthropogenic sources of ozone precursors such as NO_x and CH_4, with smaller contributions from CO and non-CH_4 VOCs. Sensitivity studies show that drastic changes to these main drivers can have large impacts on the risk to human health. However, there are also non-negligible changes due to other drivers of ozone (stratospheric ozone, aerosols and climate change), which could become more significant in the future depending on the particular emissions and climate pathway the world takes. Therefore, understanding the historical changes and drivers of ozone and human health could help to inform future policy measures.

Appendix A: Additional tables and figures

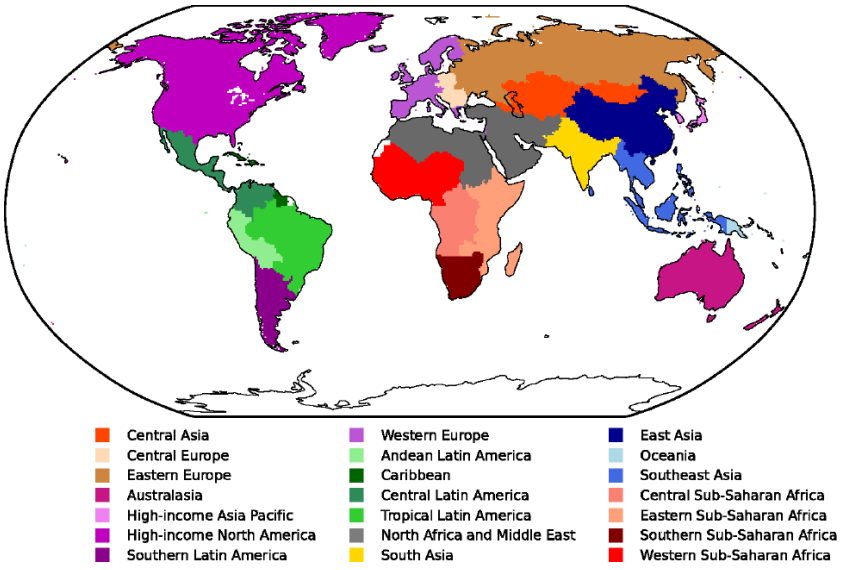

Figure A1. 21 regions used in this study based on those from the Global Burden of Disease study.

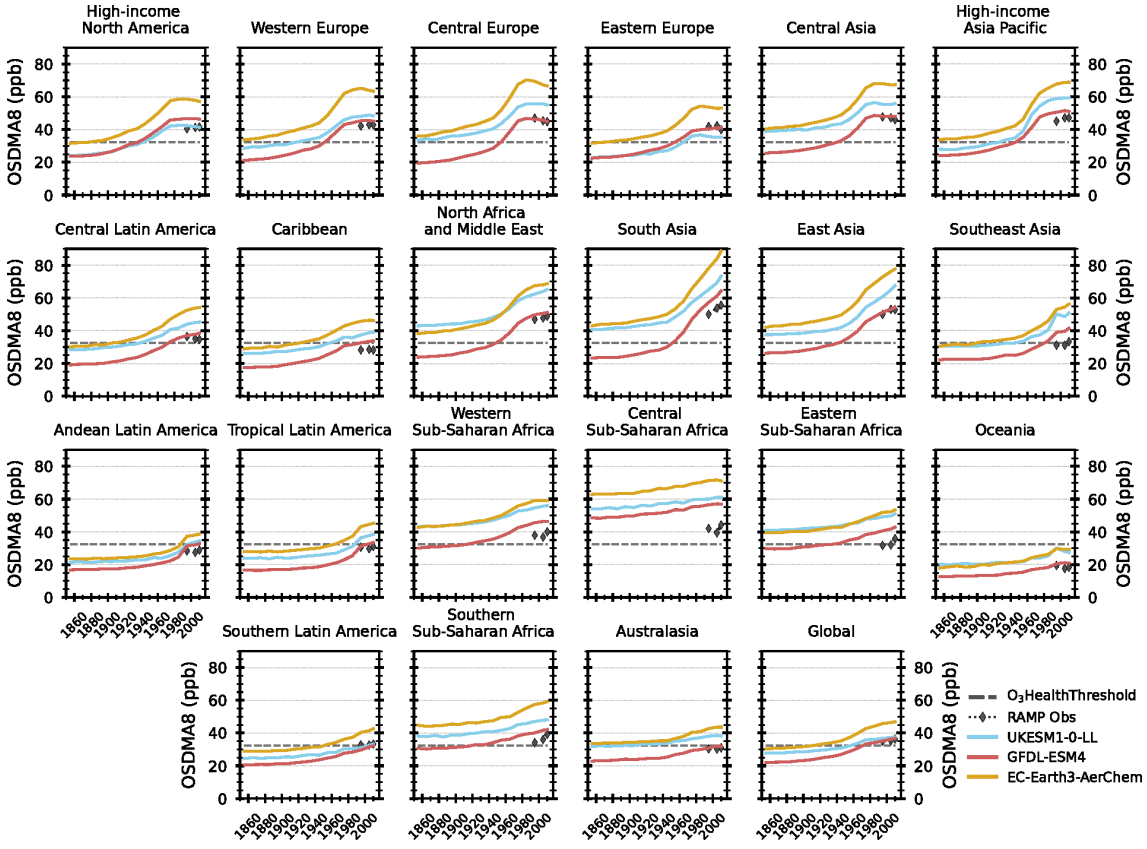

Figure A2. Uncorrected 10-year mean regional-mean surface OSDMA8 values from three CMIP6 models simulated over the historical period (1850–2014) with 10-year mean values from RAMP observations (Becker et al., 2023) shown as grey diamonds.

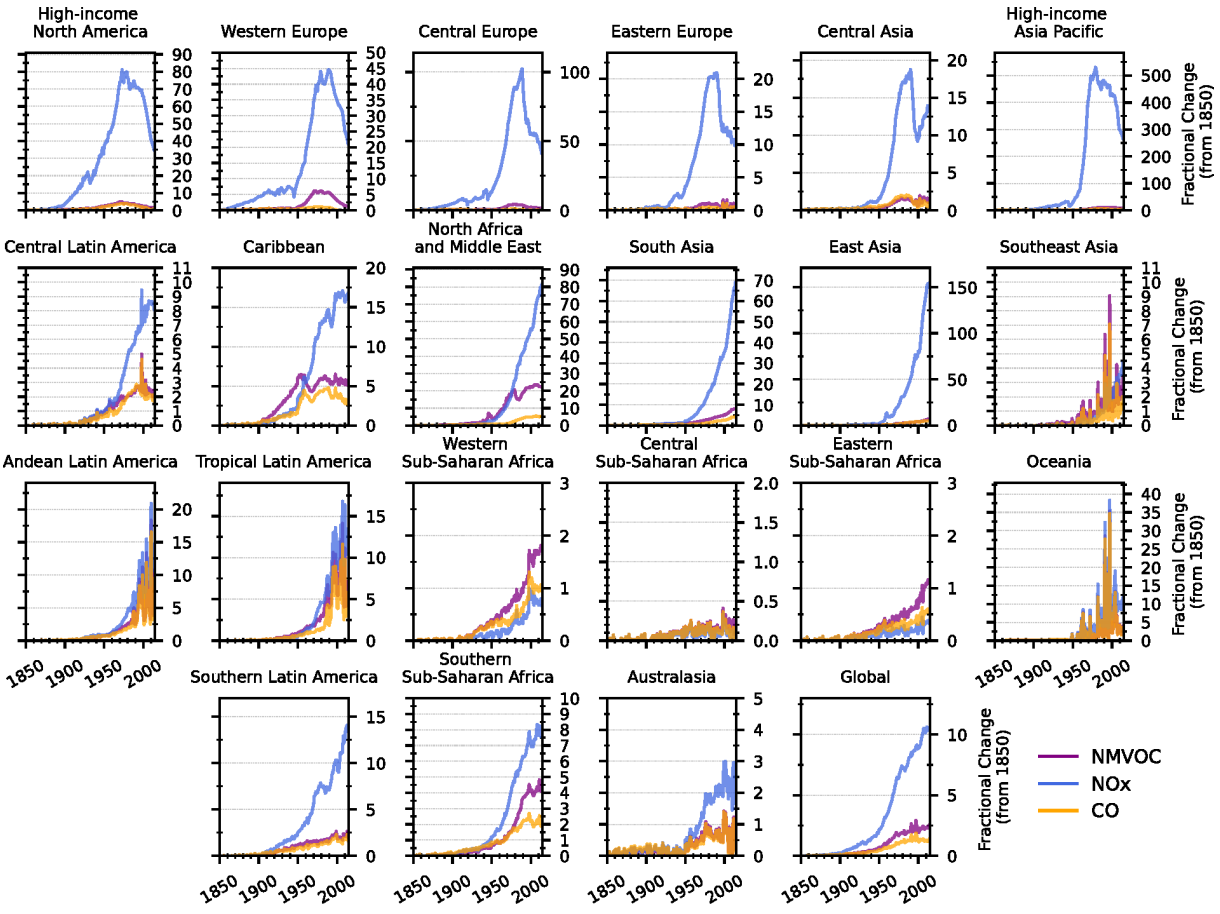

Figure A3. Relative change in historical regional emissions of ozone precursors (NO_x, CO and non-CH_4 VOCs–NMVOCs) compared to 1850 values.

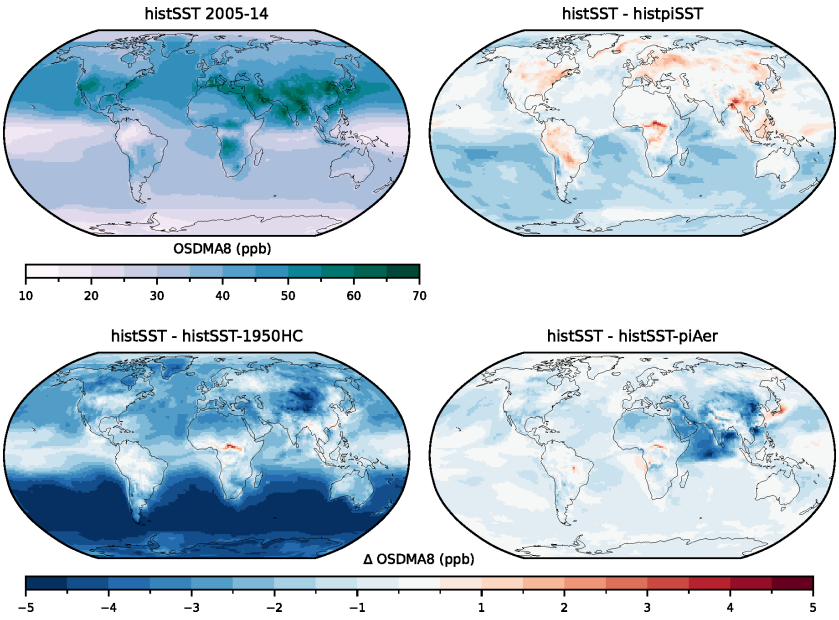

Figure A4. The 10-year mean surface OSDMA8 values simulated by UKESM1-0-LL in the HistSST experiment for 2005–2014 (bias-corrected) and the change in the same time period in the HistSST experiment relative to the histpiSST, histSST-1950HC and histSST-piAer sensitivity experiments with different drivers of ozone (climate change, stratospheric ozone and aerosols) fixed. Same information as Fig. 6 but different colour scales used.

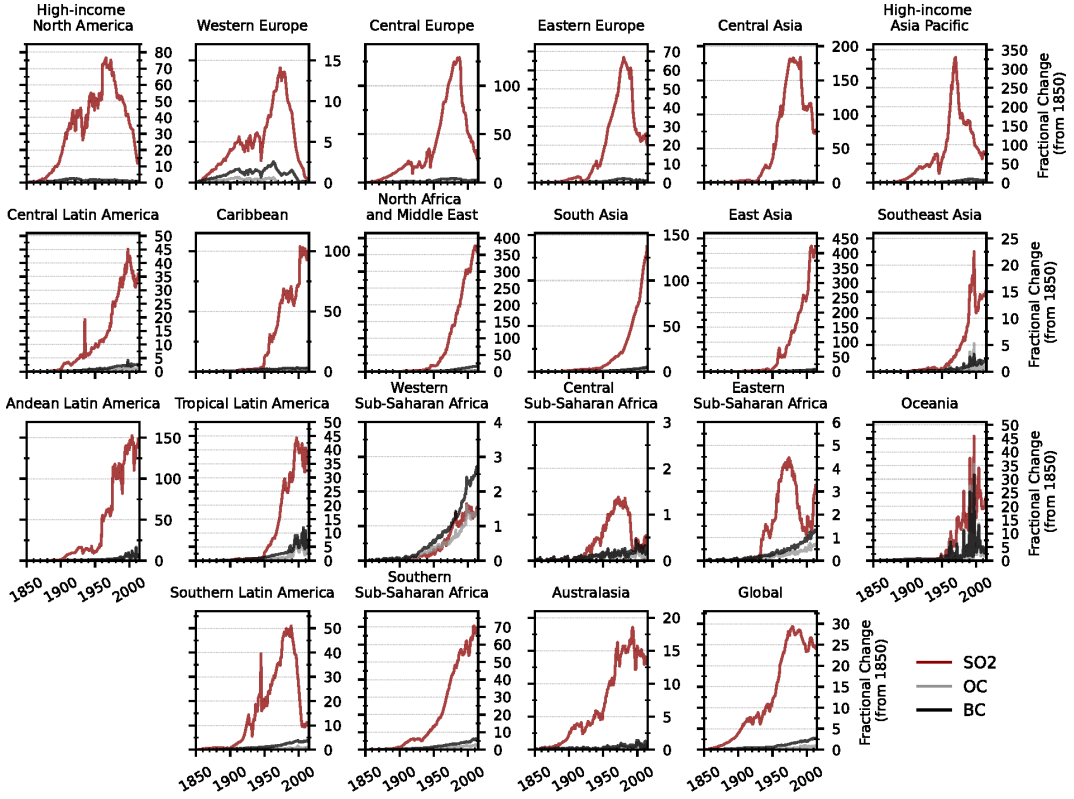

Figure A5. Relative change in historical regional emissions of ozone precursors (SO_2, OC and BC) compared to 1850 values.

Table A1. Brief description of aerosol and chemistry-relevant processes in the models used in this study.

Model	Resolution	Aerosol scheme	Chemistry scheme	Interactive elements	Reference
EC-Earth3-AerChem	Approximately 3° × 2° in horizontal (250 km) and L34 (0.1 hPa) in the vertical	M7 modal aerosol microphysical scheme for SO_4, BC, OA, sea salt and mineral dust in four soluble and three insoluble modes. NH_4, NO_3 and MSA using the Equilibrium Simplified Aerosol Model (EQSAM).	TM5 chemistry scheme accounts for gas-phase, aqueous-phase and heterogeneous chemistry based on the modified version of the CB05 carbon-bond mechanism.	Biogenic emissions of VOCs and CO are prescribed using monthly estimates from the MEGAN-MACC dataset for the year 2000. Online emissions of mineral dust and sea salt, the oceanic source of DMS, and the production of nitrogen oxides (NO_x) by lightning. Terrestrial DMS emissions from soils and vegetation, biogenic emissions of NO_x and NH_3 from soils, oceanic emissions of CO, NMVOCs and NH_3, and SO_2 fluxes from continuously emitting volcanoes.	van Noije et al. (2021)
GFDL-ESM4	Cubed-sphere (c96) grid, with ≈ 100 km native resolution, regridded to 1.0° × 1.25° and L49 (0.01 hPa) in vertical	Bulk mass-based scheme for NH_4, SO_4, NO_3, BC, OM, sea salt and dust. Five size bins are used to represent sea salt and dust.	Interactive stratosphere–troposphere. 43 photolysis reactions, 190 gas-phase kinetic reactions and 15 heterogeneous reactions. NO_x–HO_x–O_x–chemical cycles, CO reactions, and CH_4 and NMVOC oxidation reactions.	DMS and sea salt emissions calculated online as a function of wind speed (and a prescribed DMS sea water climatology). Dust emissions coupled to interactive vegetation. Lightning NO_x calculated online as a function of convection. Online emissions of BVOCs (isoprene and monoterpenes) calculated from a prescribed vegetation cover using the MEGAN2.1 algorithm, which not only has dependence on light and temperature but also inhibits isoprene emissions based on CO_2.	Horowitz et al. (2020); Dunne et al. (2020)
UKESM1-0-LL	1.25° × 1.875° in horizontal (150 km) L85 (85 km) in vertical	GLOMAP-Mode. (modal scheme, mass and number) for SO_4, BC, OM and sea salt. Mass-based bin scheme used for mineral dust.	UKCA-coupled stratosphere–troposphere. Interactive photolysis. 84 chemical tracers. Simulates chemical cycles of O_x, HO_x and NO_x, as well as oxidation reactions of CO, CH_4 and NMVOCs. In addition, heterogeneous processes, as well as Cl and Br chemistry, are included.	Online emissions of DMS, sea salt and dust aerosols as well as emissions of primary marine organics and biogenic organic compounds. Online NO_x calculated from lightning, interactive emissions of isoprene (linked to chemistry) and monoterpenes (linked to secondary aerosols) using light and temperature, but isoprene emissions are inhibited based on CO_2.	Archibald et al. (2020b), Mulcahy et al. (2020)

Data availability. The hourly surface ozone data used in this study were obtained from the CMIP6 data archive, which is hosted at the Earth System Grid Federation and is freely available to download from https://esgf-node.llnl.gov/search/cmip6/ (last access: 19 June 2025). The references for AerChemMIP data used from GFDL-ESM4, EC-Earth3-AerChem and UKESM1-0-ll are Horowitz et al. (2018) (https://doi.org/10.22033/ESGF/CMIP6.1404), EC-Earth Consortium (2020) (https://doi.org/10.22033/ESGF/CMIP6.699) and O'Connor (2019) (https://doi.org/10.22033/ESGF/CMIP6.1561). The CMIP6 variable name sfo3 has been used from the experiments listed in Table 1. Processed model data and calculations related to human health that are used in this study can be found on Zenodo at https://doi.org/10.5281/zenodo.13385648 (Turnock, S. and Akritidis,, 2024). The RAMP surface ozone observational data are from Becker et al. (2023).

Author contributions. STT set out the conceptual idea of the research project with inputs from DA and AP. The main formal analysis, including the creation of figures, was conducted by STT and DA. Observational data and additional analysis on these data were provided by HW. Additional model data were provided by LH and PZ. STT prepared the paper with contributions of writing and editing from all co-authors.

Competing interests. At least one of the co-authors is a member of the editorial board of *Atmospheric Chemistry and Physics*. The peer-review process was guided by an independent editor, and the authors also have no other competing interests to declare.

Disclaimer. Publisher's note: Copernicus Publications remains neutral with regard to jurisdictional claims made in the text, published maps, institutional affiliations, or any other geographical representation in this paper. While Copernicus Publications makes every effort to include appropriate place names, the final responsibility lies with the authors.

Special issue statement. This article is part of the special issue "Tropospheric Ozone Assessment Report Phase II (TOAR-II) Community Special Issue (ACP/AMT/BG/GMD inter-journal SI)". It is a result of the Tropospheric Ozone Assessment Report, Phase II (TOAR-II, 2020–2024).

Acknowledgements. To evaluate the CMIP6 models, we used global model data from AerChemMIP and the Regionalized Air Quality Model Performance dataset (Becker et al., 2023).

Financial support. The contributions of Steven Turnock were funded by the Met Office Climate Science for Service Partnership (CSSP) China project under the International Science Partnerships Fund (ISPF). The contributions from Mariano Mertens were funded by the German Federal Ministry of Education and Research (funding no. 01LN2207A, IMPAC^{2}T).

Review statement. This paper was edited by John Orlando and reviewed by two anonymous referees.

References

Akritidis, D., Pozzer, A., Flemming, J., Inness, A., and Zanis, P.: A Global Climatology of Tropopause Folds in CAMS and MERRA-2 Reanalyses, J. Geophys. Res.-Atmos., 126, e2020JD034115, https://doi.org/10.1029/2020JD034115, 2021.

Akritidis, D., Bacer, S., Zanis, P., Georgoulias, A. K., Chowdhury, S., Horowitz, L. W., Naik, V., O'Connor, F. M., Keeble, J., Sager, P. L., van Noije, T., Zhou, P., Turnock, S., West, J. J., Lelieveld, J., and Pozzer, A.: Strong increase in mortality attributable to ozone pollution under a climate change and demographic scenario, Environ. Res. Lett., 19, 024041, https://doi.org/10.1088/1748-9326/ad2162, 2024.

Anenberg, S. C., Horowitz, L. W., Tong, D. Q., and West, J. J.: An Estimate of the Global Burden of Anthropogenic Ozone and Fine Particulate Matter on Premature Human Mortality Using Atmospheric Modeling, Environ. Healt Perspect., 118, 1189–1195, https://doi.org/10.1289/ehp.0901220, 2010.

Archibald, A. T., Neu, J. L., Elshorbany, Y. F., Cooper, O. R., Young, P. J., Akiyoshi, H., Cox, R. A., Coyle, M., Derwent, R. G., Deushi, M., Finco, A., Frost, G. J., Galbally, I. E., Gerosa, G., Granier, C., Griffiths, P. T., Hossaini, R., Hu, L., Jöckel, P., Josse, B., Lin, M. Y., Mertens, M., Morgenstern, O., Naja, M., Naik, V., Oltmans, S., Plummer, D. A., Revell, L. E., Saiz-Lopez, A., Saxena, P., Shin, Y. M., Shahid, I., Shallcross, D., Tilmes, S., Trickl, T., Wallington, T. J., Wang, T., Worden, H. M., and Zeng, G.: Tropospheric Ozone Assessment Report: A critical review of changes in the tropospheric ozone burden and budget from 1850 to 2100, Elementa, 8, 034, https://doi.org/10.1525/elementa.2020.034, 2020a.

Archibald, A. T., O'Connor, F. M., Abraham, N. L., Archer-Nicholls, S., Chipperfield, M. P., Dalvi, M., Folberth, G. A., Dennison, F., Dhomse, S. S., Griffiths, P. T., Hardacre, C., Hewitt, A. J., Hill, R. S., Johnson, C. E., Keeble, J., Köhler, M. O., Morgenstern, O., Mulcahy, J. P., Ordóñez, C., Pope, R. J., Rumbold, S. T., Russo, M. R., Savage, N. H., Sellar, A., Stringer, M., Turnock, S. T., Wild, O., and Zeng, G.: Description and evaluation of the UKCA stratosphere–troposphere chemistry scheme (StratTrop vn 1.0) implemented in UKESM1, Geosci. Model Dev., 13, 1223–1266, https://doi.org/10.5194/gmd-13-1223-2020, 2020b.

Archibald, A. T., Turnock, S. T., Griffiths, P. T., Cox, T., Derwent, R. G., Knote, C., and Shin, M.: On the changes in surface ozone over the twenty-first century: sensitivity to changes in surface temperature and chemical mechanisms, Philos. T. Roy. Soc. A, 378, 20190329, https://doi.org/10.1098/rsta.2019.0329, 2020c.

Becker, J. S., DeLang, M. N., Chang, K.-L., Serre, M. L., Cooper, O. R., Wang, H., Schultz, M. G., Schröder, S., Lu, X., Zhang, L., Deushi, M., Josse, B., Keller, C. A., Lamarque, J.-F., Lin, M., Liu, J., Marécal, V., Strode, S. A., Sudo, K., Tilmes, S., Zhang, L., Brauer, M., and West, J. J.: Using Regionalized Air Quality Model Performance and Bayesian Maximum Entropy data fusion to map global surface ozone concentration, Elementa, 11, 00025, https://doi.org/10.1525/elementa.2022.00025, 2023.

Chen, D., Rojas, M., Samset, B., Cobb, K., Diongue Niang, A., Edwards, P., Emori, S., Faria, S., Hawkins, E., Hope, P., Huybrechts, P., Meinshausen, M., Mustafa, S., Plattner, G.-K., and Tréguier, A.-M.: Framing, Context, and Methods in Climate Change 2021: The Physical Science Basis: Working Group I Contribution to the Sixth Assessment Report of the Intergovernmental Panel on Climate Change, Cambridge University Press, 147–286, https://doi.org/10.1017/9781009157896.003, 2021.

Chen, Z., Liu, J., Qie, X., Cheng, X., Yang, M., Shu, L., and Zang, Z.: Stratospheric influence on surface ozone pollution in China, Nat. Commun., 15, 4064, https://doi.org/10.1038/s41467-024-48406-x, 2024.

Cohen, A. J., Anderson, H. R., Ostro, B., Pandey, K. D., Krzyzanowski, M., Künzli, N., Gutschmidt, K., Pope, A., Romieu, I., Samet, J. M., and Smith, K.: The Global Burden of Disease Due to Outdoor Air Pollution, J. Toxicol. Environm. Health Pt. A, 68, 1301–1307, https://doi.org/10.1080/15287390590936166, 2005.

Cohen, A. J., Brauer, M., Burnett, R., Anderson, H. R., Frostad, J., Estep, K., Balakrishnan, K., Brunekreef, B., Dandona, L., Dandona, R., Feigin, V., Freedman, G., Hubbell, B., Jobling, A., Kan, H., Knibbs, L., Liu, Y., Martin, R., Morawska, L., Pope, C. A., Shin, H., Straif, K., Shaddick, G., Thomas, M., van Dingenen, R., van Donkelaar, A., Vos, T., Murray, C. J. L., and Forouzanfar, M. H.: Estimates and 25-year trends of the global burden of disease attributable to ambient air pollution: an analysis of data from the Global Burden of Diseases Study 2015, Lancet, 389, 1907–1918, https://doi.org/10.1016/S0140-6736(17)30505-6, 2017.

Collins, W. J., Lamarque, J.-F., Schulz, M., Boucher, O., Eyring, V., Hegglin, M. I., Maycock, A., Myhre, G., Prather, M., Shindell, D., and Smith, S. J.: AerChemMIP: quantifying the effects of chemistry and aerosols in CMIP6, Geosci. Model Dev., 10, 585–607, https://doi.org/10.5194/gmd-10-585-2017, 2017.

Dahlmann, K., Grewe, V., Ponater, M., and Matthes, S.: Quantifying the contributions of individual NO_x sources to the trend in ozone radiative forcing, Atmos. Environ., 45, 2860–2868, https://doi.org/10.1016/j.atmosenv.2011.02.071, 2011.

DeLang, M. N., Becker, J. S., Chang, K.-L., Serre, M. L., Cooper, O. R., Schultz, M. G., Schröder, S., Lu, X., Zhang, L., Deushi, M., Josse, B., Keller, C. A., Lamarque, J.-F., Lin, M., Liu, J., Marécal, V., Strode, S. A., Sudo, K., Tilmes, S., Zhang, L., Cleland, S. E., Collins, E. L., Brauer, M., and West, J. J.: Mapping Yearly Fine Resolution Global Surface Ozone through the Bayesian Maximum Entropy Data Fusion of Observations and Model Output for 1990–2017, Environ. Sci. Technol., 55, 4389–4398, https://doi.org/10.1021/acs.est.0c07742, 2021.

Doherty, R. M., Wild, O., Shindell, D. T., Zeng, G., MacKenzie, I. A., Collins, W. J., Fiore, A. M., Stevenson, D. S., Dentener, F. J., Schultz, M. G., Hess, P., Derwent, R. G., and Keating, T. J.: Impacts of climate change on surface ozone and intercontinental ozone pollution: A multi-model study, J. Geophys. Res.-Atmos., 118, 3744–3763, https://doi.org/10.1002/jgrd.50266, 2013.

Dunne, J. P., Horowitz, L. W., Adcroft, A. J., Ginoux, P., Held, I. M., John, J. G., Krasting, J. P., Malyshev, S., Naik, V., Paulot, F., Shevliakova, E., Stock, C. A., Zadeh, N., Balaji, V., Blanton, C., Dunne, K. A., Dupuis, C., Durachta, J., Dussin, R., Gauthier, P. P. G., Griffies, S. M., Guo, H., Hallberg, R. W., Harrison, M., He, J., Hurlin, W., McHugh, C., Menzel, R., Milly, P. C. D., Nikonov, S., Paynter, D. J., Ploshay, J., Radhakrishnan, A., Rand, K., Reichl, B. G., Robinson, T., Schwarzkopf, D. M., Sentman, L. T., Underwood, S., Vahlenkamp, H., Winton, M., Wittenberg, A. T., Wyman, B., Zeng, Y., and Zhao, M.: The GFDL Earth System Model version 4.1 (GFDL-ESM 4.1): Overall coupled model description and simulation characteristics, J. Adv. Model. Earth Syst., 12, 2019ms002015, https://doi.org/10.1029/2019ms002015, 2020.

EC-Earth Consortium (EC-Earth): EC-Earth-Consortium EC-Earth3-AerChem model output prepared for CMIP6 AerChemMIP, Version.20220314, Earth System Grid Federation. [data set], https://doi.org/10.22033/ESGF/CMIP6.699, 2020.

EMEP Steering Body and Working Group on Effects of the Convention on Long-Range Transboundary Air Pollution: Towards Cleaner Air, Scientific Assessment Report 2016, edited by: Maas, R. and Grennfelt, P., https://unece.org/sites/default/files/2021-06/CLRTAP_Scientific_Assessment_Report_en.pdf (last access: 4 April 2025), 2016.

Fang, Y., Naik, V., Horowitz, L. W., and Mauzerall, D. L.: Air pollution and associated human mortality: the role of air pollutant emissions, climate change and methane concentration increases from the preindustrial period to present, Atmos. Chem. Phys., 13, 1377–1394, https://doi.org/10.5194/acp-13-1377-2013, 2013.

Fiore, A. M., Dentener, F. J., Wild, O., Cuvelier, C., Schultz, M. G., Hess, P., Textor, C., Schulz, M., Doherty, R. M., Horowitz, L. W., MacKenzie, I. A., Sanderson, M. G., Shindell, D. T., Stevenson, D. S., Szopa, S., Van Dingenen, R., Zeng, G., Atherton, C., Bergmann, D., Bey, I., Carmichael, G., Collins, W. J., Duncan, B. N., Faluvegi, G., Folberth, G., Gauss, M., Gong, S., Hauglustaine, D., Holloway, T., Isaksen, I. S. A., Jacob, D. J., Jonson, J. E., Kaminski, J. W., Keating, T. J., Lupu, A., Marmer, E., Montanaro, V., Park, R. J., Pitari, G., Pringle, K. J., Pyle, J. A., Schroeder, S., Vivanco, M. G., Wind, P., Wojcik, G., Wu, S., and Zuber, A.: Multimodel estimates of intercontinental source-receptor relationships for ozone pollution, J. Geophys. Res.-Atmos., 114, D04301, https://doi.org/10.1029/2008JD010816, 2009.

Fleming, Z. L., Doherty, R. M., von Schneidemesser, E., Malley, C. S., Cooper, O. R., Pinto, J. P., Colette, A., Xu, X., Simpson, D., Schultz, M. G., Lefohn, A. S., Hamad, S., Moolla, R., Solberg, S., and Feng, Z.: Tropospheric Ozone Assessment Report: Present-day ozone distribution and trends relevant to human health, Elementa, 6, 12, https://doi.org/10.1525/elementa.273, 2018.

Flynn, C. M. and Mauritsen, T.: On the climate sensitivity and historical warming evolution in recent coupled model ensembles, Atmos. Chem. Phys., 20, 7829–7842, https://doi.org/10.5194/acp-20-7829-2020, 2020.

Folberth, G. A., Staniaszek, Z., Archibald, A. T., Gedney, N., Griffiths, P. T., Jones, C. D., O'Connor, F. M., Parker, R. J., Sellar, A. A., and Wiltshire, A.: Description and Evaluation

of an Emission-Driven and Fully Coupled Methane Cycle in UKESM1, J. Adv. Model. Earth Syst., 14, e2021MS002982, https://doi.org/10.1029/2021MS002982, 2022.

Forouzanfar, M., Alexander, L., Anderson, H., Bachman, V., Biryukov, S., Brauer, M., Burnett, R., Casey, D., Coates, M., Cohen, A., Delwiche, K., Estep, K., Frostad, J., Astha, K., Kyu, H., Moradi-Lakeh, M., Ng, M., Slepak, E., Thomas, B., Wagner, J., Aasvang, G., Abbafati, C., Ozgoren, A., Abd-Allah, F., Abera, S., Aboyans, V., Abraham, B., Abraham, J., Abubakar, I., Abu-Rmeileh, N., Aburto, T., Achoki, T., Adelekan, A., Adofo, K., Adou, A., Adsuar, J., Afshin, A., Agardh, E., Al Khabouri, M., Al Lami, F., Alam, S., Alasfoor, D., Amini, H., Brooks, P., Havmøller, R., Iburg, K., Juel, K., Larsson, A., Narayan, K., Zhao, Y., and GBD 2013 Risk Factors Collaborators: Global, regional, and national comparative risk assessment of 79 behavioural, environmental and occupational, and metabolic risks or clusters of risks in 188 countries, 1990–2013: a systematic analysis for the Global Burden of Disease Study 2013, Lancet, 386, 2287–2323, https://doi.org/10.1016/S0140-6736(15)00128-2, 2015.

Fortems-Cheiney, A., Foret, G., Siour, G., Vautard, R., Szopa, S., Dufour, G., Colette, A., Lacressonniere, G., and Beekmann, M.: A 3 °C global RCP8.5 emission trajectory cancels benefits of European emission reductions on air quality, Nat. Commun., 8, 1–5, https://doi.org/10.1038/s41467-017-00075-9, 2017.

Fu, T.-M. and Tian, H.: Climate Change Penalty to Ozone Air Quality: Review of Current Understandings and Knowledge Gaps, Curr. Pollut. Rep., 5, 159–171, https://doi.org/10.1007/s40726-019-00115-6, 2019.

Gao, Y., Zhang, J., Yan, F., Leung, L. R., Luo, K., Zhang, Y., and Bell, M. L.: Nonlinear effect of compound extreme weather events on ozone formation over the United States, Weather Clim. Ext., 30, 100285, https://doi.org/10.1016/j.wace.2020.100285, 2020.

GBD 2021 Risk Factors Collaborators: Global burden and strength of evidence for 88 risk factors in 204 countries and 811 subnational locations, 1990–2021: a systematic analysis for the Global Burden of Disease Study 2021, Lancet, 403, 2162–2203, https://doi.org/10.1016/S0140-6736(24)00933-4, 2024.

Griffiths, P. T., Murray, L. T., Zeng, G., Shin, Y. M., Abraham, N. L., Archibald, A. T., Deushi, M., Emmons, L. K., Galbally, I. E., Hassler, B., Horowitz, L. W., Keeble, J., Liu, J., Moeini, O., Naik, V., O'Connor, F. M., Oshima, N., Tarasick, D., Tilmes, S., Turnock, S. T., Wild, O., Young, P. J., and Zanis, P.: Tropospheric ozone in CMIP6 simulations, Atmos. Chem. Phys., 21, 4187–4218, https://doi.org/10.5194/acp-21-4187-2021, 2021.

Hoesly, R. M., Smith, S. J., Feng, L., Klimont, Z., Janssens-Maenhout, G., Pitkanen, T., Seibert, J. J., Vu, L., Andres, R. J., Bolt, R. M., Bond, T. C., Dawidowski, L., Kholod, N., Kurokawa, J.-I., Li, M., Liu, L., Lu, Z., Moura, M. C. P., O'Rourke, P. R., and Zhang, Q.: Historical (1750–2014) anthropogenic emissions of reactive gases and aerosols from the Community Emissions Data System (CEDS), Geosci. Model Dev., 11, 369–408, https://doi.org/10.5194/gmd-11-369-2018, 2018.

Horowitz, L. W., Naik, V., Sentman, L., Paulot, F., Blanton, C., McHugh, C., Radhakrishnan, A., Rand, K., Vahlenkamp, H., Zadeh, N. T., Wilson, C., Ginoux, P., He, J., John, J. G., Lin, M., Paynter, D. J., Ploshay, J., Zhang, A., and Zeng, Y.: NOAA-GFDL GFDL-ESM4 model output prepared for CMIP6 AerChemMIP, Version 20180701, Earth System Grid Federation [data set], https://doi.org/10.22033/ESGF/CMIP6.1404, 2018.

Horowitz, L. W., Naik, V., Paulot, F., Ginoux, P. A., Dunne, J. P., Mao, J., Schnell, J., Chen, X., He, J., John, J. G., Lin, M., Lin, P., Malyshev, S., Paynter, D., Shevliakova, E., and Zhao, M.: The GFDL Global Atmospheric Chemistry-Climate Model AM4.1: Model Description and Simulation Characteristics, J. Adv. Mode. Earth Syst., 12, e2019MS002032, https://doi.org/10.1029/2019MS002032, 2020.

Iglesias-Suarez, F., Kinnison, D. E., Rap, A., Maycock, A. C., Wild, O., and Young, P. J.: Key drivers of ozone change and its radiative forcing over the 21st century, Atmos. Chem. Phys., 18, 6121–6139, https://doi.org/10.5194/acp-18-6121-2018, 2018.

Ivatt, P. D., Evans, M. J., and Lewis, A. C.: Suppression of surface ozone by an aerosol-inhibited photochemical ozone regime, Nat. Geosci., 15, 536–540, https://doi.org/10.1038/s41561-022-00972-9, 2022.

Johnson, C. E., Collins, W. J., Stevenson, D. S., and Derwent, R. G.: Relative roles of climate and emissions changes on future tropospheric oxidant concentrations, J. Geophys. Res.-Atmos., 104, 18631–18645, https://doi.org/10.1029/1999JD900204, 1999.

Keeble, J., Hassler, B., Banerjee, A., Checa-Garcia, R., Chiodo, G., Davis, S., Eyring, V., Griffiths, P. T., Morgenstern, O., Nowack, P., Zeng, G., Zhang, J., Bodeker, G., Burrows, S., Cameron-Smith, P., Cugnet, D., Danek, C., Deushi, M., Horowitz, L. W., Kubin, A., Li, L., Lohmann, G., Michou, M., Mills, M. J., Nabat, P., Olivié, D., Park, S., Seland, Ø., Stoll, J., Wieners, K.-H., and Wu, T.: Evaluating stratospheric ozone and water vapour changes in CMIP6 models from 1850 to 2100, Atmos. Chem. Phys., 21, 5015–5061, https://doi.org/10.5194/acp-21-5015-2021, 2021.

Klein Goldewijk, K., Beusen, A., Doelman, J., and Stehfest, E.: Anthropogenic land use estimates for the Holocene – HYDE 3.2, Earth Syst. Sci. Data, 9, 927–953, https://doi.org/10.5194/essd-9-927-2017, 2017.

Lelieveld, J. and Dentener, F. J.: What controls tropospheric ozone?, J. Geophys. Res.-Atmos., 105, 3531–3551, https://doi.org/10.1029/1999JD901011, 2000.

Lelieveld, J., Evans, J. S., Fnais, M., Giannadaki, D., and Pozzer, A.: The contribution of outdoor air pollution sources to premature mortality on a global scale, Nature, 525, 367–371, https://doi.org/10.1038/nature15371, 2015.

Lelieveld, J., Pozzer, A., Pöschl, U., Fnais, M., Haines, A., and Münzel, T.: Loss of life expectancy from air pollution compared to other risk factors: a worldwide perspective, Cardiovas. Res., 116, 1910–1917, https://doi.org/10.1093/cvr/cvaa025, 2020.

Liang, C.-K., West, J. J., Silva, R. A., Bian, H., Chin, M., Davila, Y., Dentener, F. J., Emmons, L., Flemming, J., Folberth, G., Henze, D., Im, U., Jonson, J. E., Keating, T. J., Kucsera, T., Lenzen, A., Lin, M., Lund, M. T., Pan, X., Park, R. J., Pierce, R. B., Sekiya, T., Sudo, K., and Takemura, T.: HTAP2 multi-model estimates of premature human mortality due to intercontinental transport of air pollution and emission sectors, Atmos. Chem. Phys., 18, 10497–10520, https://doi.org/10.5194/acp-18-10497-2018, 2018.

Lim, S. S., Vos, T., Flaxman, A. D., Danaei, G., Shibuya, K., Adair-Rohani, H., AlMazroa, M. A., Amann, M., Anderson, H. R., Andrews, K. G., et al.: A comparative risk assessment of burden of disease and injury attributable to 67 risk factors and risk factor clusters in 21 regions, 1990–2010: a systematic analysis for the

Global Burden of Disease Study 2010, Lancet, 380, 2224–2260, https://doi.org/10.1016/S0140-6736(12)61766-8, 2012.

Lin, M., Horowitz, L. W., Payton, R., Fiore, A. M., and Tonnesen, G.: US surface ozone trends and extremes from 1980 to 2014: quantifying the roles of rising Asian emissions, domestic controls, wildfires, and climate, Atmos. Chem. Phys., 17, 2943–2970, https://doi.org/10.5194/acp-17-2943-2017, 2017.

Malashock, D. A., DeLang, M. N., Becker, J. S., Serre, M. L., West, J. J., Chang, K.-L., Cooper, O. R., and Anenberg, S. C.: Estimates of ozone concentrations and attributable mortality in urban, peri-urban and rural areas worldwide in 2019, Environ. Res. Lett., 17, 054023, https://doi.org/10.1088/1748-9326/ac66f3, 2022.

Malley, C. S., Henze, D. K., Kuylenstierna, J. C., Vallack, H. W., Davila, Y., Anenberg, S. C., Turner, M. C., and Ashmore, M. R.: Updated global estimates of respiratory mortality in adults $\geq$ 30 years of age attributable to long-term ozone exposure, Environ. Health Perspect., 125, 087021, https://doi.org/10.1289/EHP1390, 2017.

Mertens, M., Brinkop, S., Graf, P., Grewe, V., Hendricks, J., Jöckel, P., Lanteri, A., Matthes, S., Rieger, V. S., Righi, M., and Thor, R. N.: The contribution of transport emissions to ozone mixing ratios and methane lifetime in 2015 and 2050 in the Shared Socioeconomic Pathways (SSPs), Atmos. Chem. Phys., 24, 12079–12106, https://doi.org/10.5194/acp-24-12079-2024, 2024.

Mills, G., Pleijel, H., Malley, C. S., Sinha, B., Cooper, O. R., Schultz, M. G., Neufeld, H. S., Simpson, D., Sharps, K., Feng, Z., Gerosa, G., Harmens, H., Kobayashi, K., Saxena, P., Paoletti, E., Sinha, V., and Xu, X.: Tropospheric Ozone Assessment Report: Present-day tropospheric ozone distribution and trends relevant to vegetation, Elementa, 6, 47, https://doi.org/10.1525/elementa.302, 2018.

Monks, P. S., Archibald, A. T., Colette, A., Cooper, O., Coyle, M., Derwent, R., Fowler, D., Granier, C., Law, K. S., Mills, G. E., Stevenson, D. S., Tarasova, O., Thouret, V., von Schneidemesser, E., Sommariva, R., Wild, O., and Williams, M. L.: Tropospheric ozone and its precursors from the urban to the global scale from air quality to short-lived climate forcer, Atmos. Chem. Phys., 15, 8889–8973, https://doi.org/10.5194/acp-15-8889-2015, 2015.

Morgenstern, O., Stone, K. A., Schofield, R., Akiyoshi, H., Yamashita, Y., Kinnison, D. E., Garcia, R. R., Sudo, K., Plummer, D. A., Scinocca, J., Oman, L. D., Manyin, M. E., Zeng, G., Rozanov, E., Stenke, A., Revell, L. E., Pitari, G., Mancini, E., Di Genova, G., Visioni, D., Dhomse, S. S., and Chipperfield, M. P.: Ozone sensitivity to varying greenhouse gases and ozone-depleting substances in CCMI-1 simulations, Atmos. Chem. Phys., 18, 1091–1114, https://doi.org/10.5194/acp-18-1091-2018, 2018.

Morice, C. P., Kennedy, J. J., Rayner, N. A., Winn, J. P., Hogan, E., Killick, R. E., Dunn, R. J. H., Osborn, T. J., Jones, P. D., and Simpson, I. R.: An Updated Assessment of Near-Surface Temperature Change From 1850: The HadCRUT5 Data Set, J. Geophys. Res.-Atmos., 126, e2019JD032361, https://doi.org/10.1029/2019JD032361, 2021.

Mulcahy, J. P., Johnson, C., Jones, C. G., Povey, A. C., Scott, C. E., Sellar, A., Turnock, S. T., Woodhouse, M. T., Abraham, N. L., Andrews, M. B., Bellouin, N., Browse, J., Carslaw, K. S., Dalvi, M., Folberth, G. A., Glover, M., Grosvenor, D. P., Hardacre, C., Hill, R., Johnson, B., Jones, A., Kipling, Z., Mann, G., Mollard, J., O'Connor, F. M., Palmiéri, J., Reddington, C., Rumbold, S. T., Richardson, M., Schutgens, N. A. J., Stier, P., Stringer, M., Tang, Y., Walton, J., Woodward, S., and Yool, A.: Description and evaluation of aerosol in UKESM1 and HadGEM3-GC3.1 CMIP6 historical simulations, Geosci. Model Dev., 13, 6383–6423, https://doi.org/10.5194/gmd-13-6383-2020, 2020.

Mulcahy, J. P., Jones, C. G., Rumbold, S. T., Kuhlbrodt, T., Dittus, A. J., Blockley, E. W., Yool, A., Walton, J., Hardacre, C., Andrews, T., Bodas-Salcedo, A., Stringer, M., de Mora, L., Harris, P., Hill, R., Kelley, D., Robertson, E., and Tang, Y.: UKESM1.1: development and evaluation of an updated configuration of the UK Earth System Model, Geosci. Model Dev., 16, 1569–1600, https://doi.org/10.5194/gmd-16-1569-2023, 2023.

Murray, C. J., Aravkin, A. Y., Zheng, P., Abbafati, C., Abbas, K. M., Abbasi-Kangevari, M., Abd-Allah, F., Abdelalim, A., Abdollahi, M., Abdollahpour, I., et al.: Global burden of 87 risk factors in 204 countries and territories, 1990–2019: a systematic analysis for the Global Burden of Disease Study 2019, Lancet, 396, 1223–1249, https://doi.org/10.1016/S0140-6736(20)30752-2, 2020.

O'Connor, F.: MOHC UKESM1.0-LL model output prepared for CMIP6 AerChemMIP, Version 20190902, Earth System Grid Federation [data set], https://doi.org/10.22033/ESGF/CMIP6.1561, 2019.

O'Connor, F. M., Abraham, N. L., Dalvi, M., Folberth, G. A., Griffiths, P. T., Hardacre, C., Johnson, B. T., Kahana, R., Keeble, J., Kim, B., Morgenstern, O., Mulcahy, J. P., Richardson, M., Robertson, E., Seo, J., Shim, S., Teixeira, J. C., Turnock, S. T., Williams, J., Wiltshire, A. J., Woodward, S., and Zeng, G.: Assessment of pre-industrial to present-day anthropogenic climate forcing in UKESM1, Atmos. Chem. Phys., 21, 1211–1243, https://doi.org/10.5194/acp-21-1211-2021, 2021.

Ostro, B.: Outdoor air pollution: Assessing the environmental burden of disease at national and local levels, Geneva, World Health Organization, WHO Environmental Burden of Disease Series, No. 5, https://www.who.int/publications/i/item/9241591463 (last access: 4 July 2025), 2004.

Parrish, D. D., Lamarque, J.-F., Naik, V., Horowitz, L., Shindell, D. T., Staehelin, J., Derwent, R., Cooper, O. R., Tanimoto, H., Volz-Thomas, A., Gilge, S., Scheel, H.-E., Steinbacher, M., and Fröhlich, M.: Long-term changes in lower tropospheric baseline ozone concentrations: Comparing chemistry-climate models and observations at northern midlatitudes, J. Geophys. Res.-Atmos., 119, 5719–5736, https://doi.org/10.1002/2013JD021435, 2014.

Parrish, D. D., Derwent, R. G., Turnock, S. T., O'Connor, F. M., Staehelin, J., Bauer, S. E., Deushi, M., Oshima, N., Tsigaridis, K., Wu, T., and Zhang, J.: Investigations on the anthropogenic reversal of the natural ozone gradient between northern and southern midlatitudes, Atmos. Chem. Phys., 21, 9669–9679, https://doi.org/10.5194/acp-21-9669-2021, 2021.

Pope, C. A., Burnett, R. T., Thun, M. J., Calle, E. E., Krewski, D., Ito, K., and Thurston, G. D.: Lung Cancer, Cardiopulmonary Mortality, and Long-term Exposure to Fine Particulate Air Pollution, JAMA, 287, 1132–1141, https://doi.org/10.1001/jama.287.9.1132, 2002.

Pozzer, A., Anenberg, S. C., Dey, S., Haines, A., Lelieveld, J., and Chowdhury, S.: Mortality Attributable to Ambient Air Pollution: A Review of Global Estimates, GeoHealth, 7, e2022GH000711, https://doi.org/10.1029/2022GH000711, 2023.

Pozzer, A., Steffens, B., Proestos, Y., Sciare, J., Akritidis, D., Chowdhury, S., Burkart, K., and Bacer, S.: Atmospheric health

burden across the century and the accelerating impact of temperature compared to pollution, Nat. Commun., 15, 9379, https://doi.org/10.1038/s41467-024-53649-9, 2024.

Prather, M. J.: Time scales in atmospheric chemistry: Theory, GWPs for CH_4 and CO, and runaway growth, Geophys. Res. Lett., 23, 2597–2600, https://doi.org/10.1029/96GL02371, 1996.

Qu, Y., Voulgarakis, A., Wang, T., Kasoar, M., Wells, C., Yuan, C., Varma, S., and Mansfield, L.: A study of the effect of aerosols on surface ozone through meteorology feedbacks over China, Atmos. Chem. Phys., 21, 5705–5718, https://doi.org/10.5194/acp-21-5705-2021, 2021.

Rowlinson, M. J., Rap, A., Hamilton, D. S., Pope, R. J., Hantson, S., Arnold, S. R., Kaplan, J. O., Arneth, A., Chipperfield, M. P., Forster, P. M., and Nieradzik, L.: Tropospheric ozone radiative forcing uncertainty due to pre-industrial fire and biogenic emissions, Atmos. Chem. Phys., 20, 10937–10951, https://doi.org/10.5194/acp-20-10937-2020, 2020.

Schnell, J. L., Prather, M. J., Josse, B., Naik, V., Horowitz, L. W., Zeng, G., Shindell, D. T., and Faluvegi, G.: Effect of climate change on surface ozone over North America, Europe, and East Asia, Geophys. Res. Lett., 43, 3509–3518, https://doi.org/10.1002/2016GL068060, 2016.

Sellar, A. A., Jones, C. G., Mulcahy, J., Tang, Y., Yool, A., Wiltshire, A., O'Connor, F. M., Stringer, M., Hill, R., Palmieri, J., Woodward, S., Mora, L., Kuhlbrodt, T., Rumbold, S., Kelley, D. I., Ellis, R., Johnson, C. E., Walton, J., Abraham, N. L., Andrews, M. B., Andrews, T., Archibald, A. T., Berthou, S., Burke, E., Blockley, E., Carslaw, K., Dalvi, M., Edwards, J., Folberth, G. A., Gedney, N., Griffiths, P. T., Harper, A. B., Hendry, M. A., Hewitt, A. J., Johnson, B., Jones, A., Jones, C. D., Keeble, J., Liddicoat, S., Morgenstern, O., Parker, R. J., Predoi, V., Robertson, E., Siahaan, A., Smith, R. S., Swaminathan, R., Woodhouse, M. T., Zeng, G., and Zerroukat, M.: UKESM1: Description and evaluation of the UK Earth System Model, J. Adv. Model. Earth Syst., 11, 4513–4558, https://doi.org/10.1029/2019MS001739, 2019.

Sellar, A. A., Walton, J., Jones, C. G., Wood, R., Abraham, N. L., Andrejczuk, M., Andrews, M. B., Andrews, T., Archibald, A. T., de Mora, L., Dyson, H., Elkington, M., Ellis, R., Florek, P., Good, P., Gohar, L., Haddad, S., Hardiman, S. C., Hogan, E., Iwi, A., Jones, C. D., Johnson, B., Kelley, D. I., Kettleborough, J., Knight, J. R., Köhler, M. O., Kuhlbrodt, T., Liddicoat, S., Linova-Pavlova, I., Mizielinski, M. S., Morgenstern, O., Mulcahy, J., Neininger, E., O'Connor, F. M., Petrie, R., Ridley, J., Rioual, J. C., Roberts, M., Robertson, E., Rumbold, S., Seddon, J., Shepherd, H., Shim, S., Stephens, A., Teixiera, J. C., Tang, Y., Williams, J., Wiltshire, A., and Griffiths, P. T.: Implementation of U.K. Earth System Models for CMIP6, J. Adv. Model. Earth Syst., 12, 1–27, https://doi.org/10.1029/2019MS001946, 2020.

Silva, R. A., West, J. J., Zhang, Y., Anenberg, S. C., Lamarque, J.-F., Shindell, D. T., Collins, W. J., Dalsoren, S., Faluvegi, G., Folberth, G., Horowitz, L. W., Nagashima, T., Naik, V., Rumbold, S., Skeie, R., Sudo, K., Takemura, T., Bergmann, D., Cameron-Smith, P., Cionni, I., Doherty, R. M., Eyring, V., Josse, B., MacKenzie, I. A., Plummer, D., Righi, M., Stevenson, D. S., Strode, S., Szopa, S., and Zeng, G.: Global premature mortality due to anthropogenic outdoor air pollution and the contribution of past climate change, Environ. Res. Lett., 8, 034005, https://doi.org/10.1088/1748-9326/8/3/034005, 2013.

Silva, R. A., West, J. J., Lamarque, J.-F., Shindell, D. T., Collins, W. J., Dalsoren, S., Faluvegi, G., Folberth, G., Horowitz, L. ., Nagashima, T., Naik, V., Rumbold, S. T., Sudo, K., Takemura, T., Bergmann, D., Cameron-Smith, P., Cionni, I., Doherty, R. M., Eyring, V., Josse, B., MacKenzie, I. A., Plummer, D., Righi, M., Stevenson, D. S., Strode, S., Szopa, S., and Zengast, G.: The effect of future ambient air pollution on human premature mortality to 2100 using output from the ACCMIP model ensemble, Atmos. Chem. Phys., 16, 9847–9862, https://doi.org/10.5194/acp-16-9847-2016, 2016.

Škerlak, B., Sprenger, M., and Wernli, H.: A global climatology of stratosphere–troposphere exchange using the ERA-Interim data set from 1979 to 2011, Atmos. Chem. Phys., 14, 913–937, https://doi.org/10.5194/acp-14-913-2014, 2014.

Staehle, C., Rieder, H. E., Fiore, A. M., and Schnell, J. L.: Technical note: An assessment of the performance of statistical bias correction techniques for global chemistry–climate model surface ozone fields, Atmos. Chem. Phys., 24, 5953–5969, https://doi.org/10.5194/acp-24-5953-2024, 2024.

Stevenson, D. S., Young, P. J., Naik, V., Lamarque, J.-F., Shindell, D. T., Voulgarakis, A., Skeie, R. B., Dalsoren, S. B., Myhre, G., Berntsen, T. K., Folberth, G. A., Rumbold, S. T., Collins, W. J., MacKenzie, I. A., Doherty, R. M., Zeng, G., van Noije, T. P. C., Strunk, A., Bergmann, D., Cameron-Smith, P., Plummer, D. A., Strode, S. A., Horowitz, L., Lee, Y. H., Szopa, S., Sudo, K., Nagashima, T., Josse, B., Cionni, I., Righi, M., Eyring, V., Conley, A., Bowman, K. W., Wild, O., and Archibald, A.: Tropospheric ozone changes, radiative forcing and attribution to emissions in the Atmospheric Chemistry and Climate Model Intercomparison Project (ACCMIP), Atmos. Chem. Phys., 13, 3063—3085, https://doi.org/10.5194/acp-13-3063-2013, 2013.

Stevenson, D. S., Zhao, A., Naik, V., O'Connor, F. M., Tilmes, S., Zeng, G., Murray, L. T., Collins, W. J., Griffiths, P. T., Shim, S., Horowitz, L. W., Sentman, L. T., and Emmons, L.: Trends in global tropospheric hydroxyl radical and methane lifetime since 1850 from AerChemMIP, Atmos. Chem. Phys., 20, 12905–12920, https://doi.org/10.5194/acp-20-12905-2020, 2020.

Stohl, A., Bonasoni, P., Cristofanelli, P., Collins, W., Feichter, J., Frank, A., Forster, C., Gerasopoulos, E., Gäggeler, H., James, P., Kentarchos, T., Kromp-Kolb, H., Krüger, B., Land, C., Meloen, J., Papayannis, A., Priller, A., Seibert, P., Sprenger, M., Roelofs, G. J., Scheel, H. E., Schnabel, C., Siegmund, P., Tobler, L., Trickl, T., Wernli, H., Wirth, V., Zanis, P., and Zerefos, C.: Stratosphere-troposphere exchange: A review, and what we have learned from STACCATO, J. Geophys. Res.-Atmos., 108, 8516, https://doi.org/10.1029/2002JD002490, 2003.

Szopa, S., Naik, V., Adhikar, B., Artaxo, P., Berntsen, T., Collins, W., Fuzzi, S., Gallardo, L., Kiendler-Scharr, A., Klimont, Z., Liao, H., Unger, N., and Zanis, P.: Short-lived Climate Forcersin Climate Change 2021: The Physical Science Basis: Working Group I Contribution to the Sixth Assessment Report of the Intergovernmental Panel on Climate Change, Cambridge University Press, 817–922, https://doi.org/10.1017/9781009157896.008, 2021.

Tarasick, D., Galbally, I. E., Cooper, O. R., Schultz, M. G., Ancellet, G., Leblanc, T., Wallington, T. J., Ziemke, J., Liu, X., Steinbacher, M., Staehelin, J., Vigouroux, C., Hannigan, J. W., García, O., Foret, G., Zanis, P., Weatherhead, E., Petropavlovskikh, I., Worden, H., Osman, M., Liu, J., Chang,

K.-L., Gaudel, A., Lin, M., Granados-Muñoz, M., Thompson, A. M., Oltmans, S. J., Cuesta, J., Dufour, G., Thouret, V., Hassler, B., Trickl, T., and Neu, J. L.: Tropospheric Ozone Assessment Report: Tropospheric ozone from 1877 to 2016, observed levels, trends and uncertainties, Elementa, 7, 39, https://doi.org/10.1525/elementa.376, 2019.

Turnock, S. and Akritidis, D.: Dataset for Drivers of change in Peak Season Surface Ozone Concentrations and Impacts on Human Health over the Historical Period (1850–2014), Zenodo [data set], https://doi.org/10.5281/zenodo.13385648, 2024.

Turnock, S. T., Spracklen, D. V., Carslaw, K. S., Mann, G. W., Woodhouse, M. T., Forster, P. M., Haywood, J., Johnson, C. E., Dalvi, M., Bellouin, N., and Sanchez-Lorenzo, A.: Modelled and ob 1960 and 2009, Atmos. Chem. Phys., 15, 9477–9500, https://doi.org/10.5194/acp-15-9477-2015, 2015.

Turnock, S. T., Wild, O., Dentener, F. J., Davila, Y., Emmons, L. K., Flemming, J., Folberth, G. A., Henze, D. K., Jonson, J. E., Keating, T. J., Kengo, S., Lin, M., Lund, M., Tilmes, S., and O'Connor, F. M.: The impact of future emission policies on tropospheric ozone using a parameterised approach, Atmos. Chem. Phys., 18, 8953–8978, https://doi.org/10.5194/acp-18-8953-2018, 2018.

Turnock, S. T., Allen, R. J., Andrews, M., Bauer, S. E., Deushi, M., Emmons, L., Good, P., Horowitz, L., John, J. G., Michou, M., Nabat, P., Naik, V., Neubauer, D., O'Connor, F. M., Olivié, D., Oshima, N., Schulz, M., Sellar, A., Shim, S., Takemura, T., Tilmes, S., Tsigaridis, K., Wu, T., and Zhang, J.: Historical and future changes in air pollutants from CMIP6 models, Atmos. Chem. Phys., 20, 14547–14579, https://doi.org/10.5194/acp-20-14547-2020, 2020.

Turnock, S. T., Reddington, C. L., West, J. J., and O'Connor, F. M.: The Air Pollution Human Health Burden in Different Future Scenarios That Involve the Mitigation of Near-Term Climate Forcers, Climate and Land-Use, GeoHealth, 7, e2023GH000812, https://doi.org/10.1029/2023GH000812, 2023.

United Nations Economic Commission for Europe: Clearing the Air: 25 years of the Convention on Long-Range Transboundary Air Pollution, ISBN 9211169100, https://unece.org/sites/default/files/2021-06/25thyearanniversaryBOOKscreen.pdf (last access: 28 February 2020), 2004.

van Noije, T., Bergman, T., Le Sager, P., O'Donnell, D., Makkonen, R., Gonçalves-Ageitos, M., Döscher, R., Fladrich, U., von Hardenberg, J., Keskinen, J.-P., Korhonen, H., Laakso, A., Myriokefalitakis, S., Ollinaho, P., Pérez García-Pando, C., Reerink, T., Schrödner, R., Wyser, K., and Yang, S.: EC-Earth3-AerChem: a global climate model with interactive aerosols and atmospheric chemistry participating in CMIP6, Geosci. Model Dev., 14, 5637–5668, https://doi.org/10.5194/gmd-14-5637-2021, 2021.

Wang, H., Lu, X., Jacob, D. J., Cooper, O. R., Chang, K.-L., Li, K., Gao, M., Liu, Y., Sheng, B., Wu, K., Wu, T., Zhang, J., Sauvage, B., Nédélec, P., Blot, R., and Fan, S.: Global tropospheric ozone trends, attributions, and radiative impacts in 1995–2017: an integrated analysis using aircraft (IAGOS) observations, ozonesonde, and multi-decadal chemical model simulations, Atmos. Chem. Phys., 22, 13753–13782, https://doi.org/10.5194/acp-22-13753-2022, 2022.

West, J. J., Szopa, S., and Hauglustaine, D. A.: Human mortality effects of future concentrations of tropospheric ozone, Comptes Rendus Geoscience, 339, 775–783, https://doi.org/10.1016/j.crte.2007.08.005, 2007.

Wild, O. and Prather, M. J.: Global tropospheric ozone modeling: Quantifying errors due to grid resolution, J. Geophys. Res.-Atmos., 111, D11305, https://doi.org/10.1029/2005JD006605, 2006.

Wild, O., Fiore, A. M., Shindell, D. T., Doherty, R. M., Collins, W. J., Dentener, F. J., Schultz, M. G., Gong, S., MacKenzie, I. A., Zeng, G., Hess, P., Duncan, B. N., Bergmann, D. J., Szopa, S., Jonson, J. E., Keating, T. J., and Zuber, A.: Modelling future changes in surface ozone: a parameterized approach, Atmos. Chem. Phys., 12, 2037–2054, https://doi.org/10.5194/acp-12-2037-2012, 2012.

Wild, O., Voulgarakis, A., O'Connor, F., Lamarque, J.-F., Ryan, E. M., and Lee, L.: Global sensitivity analysis of chemistry–climate model budgets of tropospheric ozone and OH: exploring model diversity, Atmos. Chem. Phys., 20, 4047–4058, https://doi.org/10.5194/acp-20-4047-2020, 2020.

Xing, J., Wang, J., Mathur, R., Wang, S., Sarwar, G., Pleim, J., Hogrefe, C., Zhang, Y., Jiang, J., Wong, D. C., and Hao, J.: Impacts of aerosol direct effects on tropospheric ozone through changes in atmospheric dynamics and photolysis rates, Atmos. Chem. Phys., 17, 9869–9883, https://doi.org/10.5194/acp-17-9869-2017, 2017.

Yan, Y., Pozzer, A., Ojha, N., Lin, J., and Lelieveld, J.: Analysis of European ozone trends in the period 1995–2014, Atmos. Chem. Phys., 18, 5589–5605, https://doi.org/10.5194/acp-18-5589-2018, 2018.

Young, P. J., Archibald, A. T., Bowman, K. W., Lamarque, J.-F., Naik, V., Stevenson, D. S., Tilmes, S., Voulgarakis, A., Wild, O., Bergmann, D., Cameron-Smith, P., Cionni, I., Collins, W. J., Dalsøren, S. B., Doherty, R. M., Eyring, V., Faluvegi, G., Horowitz, L. W., Josse, B., Lee, Y. H., MacKenzie, I. A., Nagashima, T., Plummer, D. A., Righi, M., Rumbold, S. T., Skeie, R. B., Shindell, D. T., Strode, S. A., Sudo, K., Szopa, S., and Zeng, G.: Preindustrial to end 21st century projections of tropospheric ozone from the Atmospheric Chemistry and Climate Model Intercomparison Project (ACCMIP), Atmos. Chem. Phys., 13, 2063–2090, https://doi.org/10.5194/acp-13-2063-2013, 2013.

Young, P. J., Naik, V., Fiore, A. M., Gaudel, A., Guo, J., Lin, M. Y., Neu, J. L., Parrish, D. D., Rieder, H. E., Schnell, J. L., Tilmes, S., Wild, O., Zhang, L., Ziemke, J. R., Brandt, J., Delcloo, A., Doherty, R. M., Geels, C., Hegglin, M. I., Hu, L., Im, U., Kumar, R., Luhar, A., Murray, L., Plummer, D., Rodriguez, J., Saiz-Lopez, A., Schultz, M. G., Woodhouse, M. T., and Zeng, G.: Tropospheric Ozone Assessment Report: Assessment of global-scale model performance for global and regional ozone distributions, variability, and trends, Elem. Sci. Anth., 6, 10, https://doi.org/10.1525/elementa.265, 2018.

Zanis, P., Akritidis, D., Turnock, S., Naik, V., Szopa, S., Georgoulias, A. K., Bauer, S. E., Deushi, M., Horowitz, L. W., Keeble, J., Sager, P. L., O'Connor, F. M., Oshima, N., Tsigaridis, K., and van Noije, T.: Climate change penalty and benefit on surface ozone: A global perspective based on CMIP6 earth system models, Environ. Res. Lett., 17, 024014, https://doi.org/10.1088/1748-9326/ac4a34, 2022.

Zeng, G., Morgenstern, O., Williams, J. H. T., O'Connor, F. M., Griffiths, P. T., Keeble, J., Deushi, M., Horowitz, L. W., Naik, V., Emmons, L. K., Abraham, N. L., Archibald, A. T.,

Bauer, S. E., Hassler, B., Michou, M., Mills, M. J., Murray, L. T., Oshima, N., Sentman, L. T., Tilmes, S., Tsigaridis, K., and Young, P. J.: Attribution of Stratospheric and Tropospheric Ozone Changes Between 1850 and 2014 in CMIP6 Models, J. Geophys. Res.-Atmos., 127, e2022JD036452, https://doi.org/10.1029/2022JD036452, 2022.

Zhang, J., Furtado, K., Turnock, S. T., Mulcahy, J. P., Wilcox, L. J., Booth, B. B., Sexton, D., Wu, T., Zhang, F., and Liu, Q.: The role of anthropogenic aerosols in the anomalous cooling from 1960 to 1990 in the CMIP6 Earth system models, Atmos. Chem. Phys., 21, 18609–18627, https://doi.org/10.5194/acp-21-18609-2021, 2021.

Zhang, Y., Cooper, O. R., Gaudel, A., Thompson, A. M., Nédélec, P., Ogino, S.-Y., and West, J. J.: Tropospheric ozone change from 1980 to 2010 dominated by equatorward redistribution of emissions, Nat. Geosci., 9, 875–879, https://doi.org/10.1038/ngeo2827, 2016.